CONSORTIUM FOR MATERIALS DEVELOPMENT IN SPACE

ANNUAL REPORT
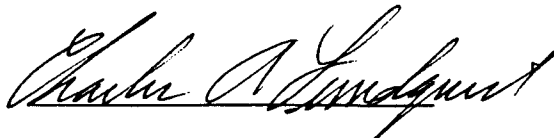
Technical Section

SEP 15, '86 — SEP 14, '87

NAGW—812

Submitted by The University of Alabama in Huntsville,
the legal entity responsible for establishing the Consortium.

Submitted to Market Development Branch,
Commercial Development Division,
Office of Commercial Programs
National Aeronautics and Space Administration
Washington, D.C.

Industrial Members: Boeing Aerospace Corporation
Deere & Company
Martin Marietta Denver Aerospace
McDonnell Douglas Astronautics Co. - Huntsville
Teledyne Brown Engineering
Wyle Laboratories

Charles A. Lundquist
Director, CMDS

TABLE OF CONTENTS

i

I. INTRODUCTION AND SCOPE

This report for the fiscal year 1987, covers for each CMDS project (and task) its status as of September 14. It does not address plans for space flights of the equipment associated with each project; a previous quarterly report discussed a flight experiment model. The model needs revision based on more specific manifest plans announced by NASA. This revision will be addressed in a future quarterly report.

Table 1 lists the current projects and tasks and gives a few points of basic information on each (see also Ref. 1). The table serves as a summary and guide to the more detailed sections that follow.

A number of discussions are now underway with potential new industrial members of the CMDS. Completion of these discussions is predicated in part on clarification of prospects for flight assignments. Naturally, new members will wish to understand the flight opportunities and plans attached to the project or task they would join. IBM's Almaden Research Center has agreed to joint research on the Highly Non-Linear Optical Organic Crystals Project. Consideration of this as a Consortium effort will be an agenda topic for the Council in its meeting during the first quarter of FY 1988.

The High Temperature Superconductors Project deserves individual mention. It is based on a breakthrough in higher temperature superconducting materials. See Appendix I for a copy of the discovery paper. The first material to exhibit superconductivity above liquid nitrogen temperatures was produced and tested in laboratories at UAH by Dr. M. K. Wu and his associates. This work was supported in part by the CMDS. The industrial implications of these new materials are expected to be great. Among the many expected applications will be superconducting devices that advance the capabilities of commercial satellites. Communication satellites are perhaps the earliest prospect. For this project,

1

TABLE 1

PROJECT OR TASK	STATUS	INDUSTRIAL PARTICIPANT	POTENTIAL PRODUCT	ATTRIBUTE OF SPACE USED	REMARKS
Physical Vapor Transport Crystal Growth	Original Project	Boeing Aerospace Corporation	Zinc selenide electro-optical devices	Microgravity	Gram size crystals being grown in preflight laboratory hardware
Materials Preparation and Longevity in Hyperthermal Atomic Oxygen	Original Project	Martin Marietta Denver Aerospace	Spacecraft surface coatings	Flux of Atomic Oxygen	Arrhenius activation energies and particle accommodation calculated from previous flight data
Surface Coatings and Catalyst Production by Electrodeposition	Original Project	McDonnell Douglas Astronautics Co., Huntsville	Improved surface coatings and metal catalysts	Microgravity	Flight equipment successfully used on KC-135 tests
Highly Non-linear Optical Organic Crystals and Films	Original Projects	Formerly Celanese Research Company and GTE	Optical computers and electrooptical devices	Microgravity	Important theoretical advances. Flight equipment redesigned
Physical Properties of Immiscible Polymers	Original Project, restructuring begun	Originally Union Carbide and Subsequently Celanese	Blended polymers and separation of organic materials	Microgravity	Flight equipment successfully used on KC-135 tests

2

PROJECT OR TASK	STATUS	INDUSTRIAL PARTICIPANT	POTENTIAL PRODUCT	ATTRIBUTE OF SPACE USED	REMARKS
High Temperature Superconductors	New Project	To be determined during FY 1988	Improved systems for commercial spacecraft	Radiation heat-sink of space	Major breakthrough in FY 1987
Powdered Metal Sintering	Original Task	Teledyne Brown Engineering	Metal-ceramic mixtures	Microgravity	1900 C ground based directional furnace completed
Iron-Carbon Solidification	Original Task	Deere and Company	Improved cast iron processes	Microgravity	Mature laboratory capability
Wake Shield	Original Task	Wyle Laboratories	Purified materials	Vacuum volume with equivalent of high-pumping rate	Flow fields investigated

FY 1988 must be a year of definition and identification of industrial members. As currently envisioned, the need for flight experiments for this project will not be as immediate as for the others.

The Consortium organization and mode of operation remains essentially the organization chart reproduced below. The principle activities of the Consortium are concentrated in the Projects. Activities currently having lesser scope are designated, Tasks. Some of these will eventually evolve into Projects.
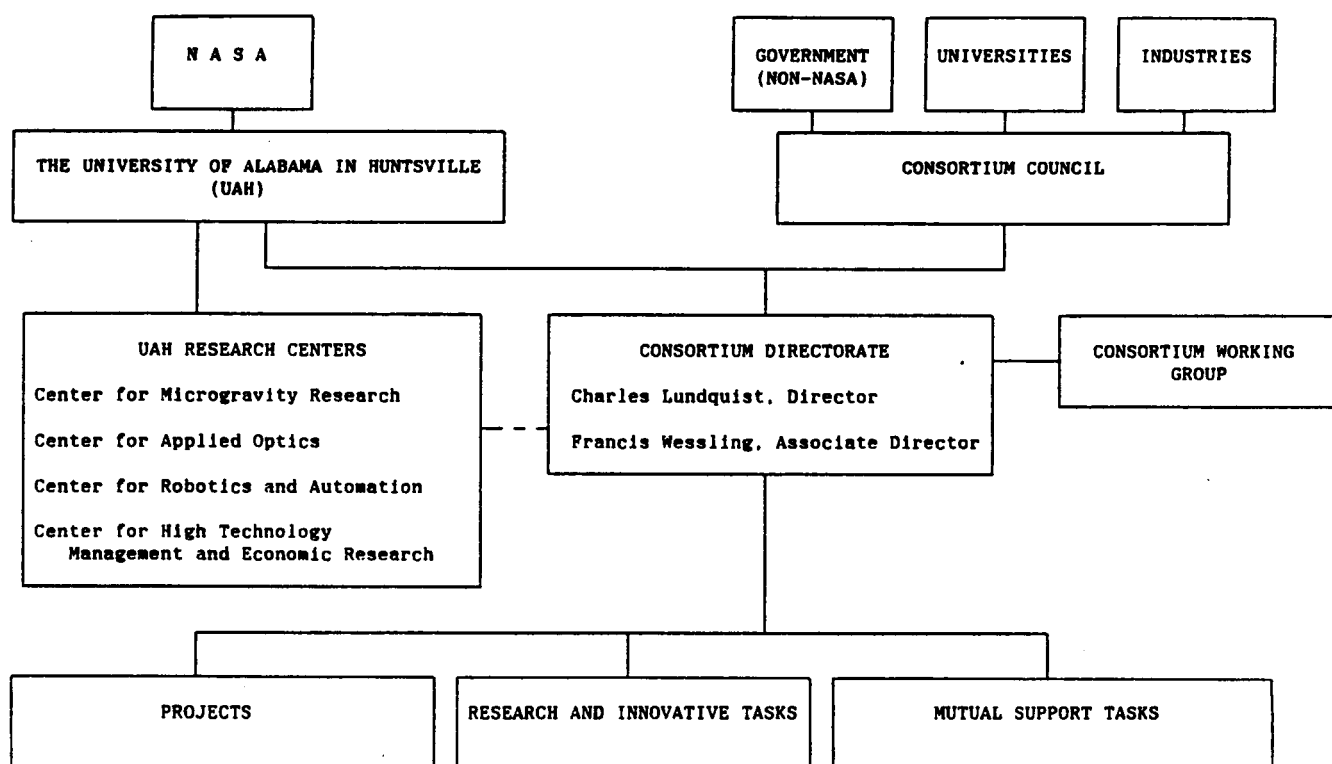
References

1. Lundquist, C. A., <u>Mat. Res. Soc. Symp. Proc.</u> Vol. 87, pp. 121-127 (1987).

II. PROJECTS

Center: Consortium for Materials Development in Space
         The University of Alabama in Hunstville (UAH)

Project Name: **"Physical Vapor Transport Crystal Growth"**

Industrial Participant: Boeing Aerospace Company (BAC)
                           Seattle, WA 98124
                           Dave W. Yoel

The University of Alabama in Huntsville
                           Elmer Anderson
                           Maw-Kuen Wu
                           H. Y. Cheng

Annual Report: September 15, 1986 to September 14, 1987

* *

Introduction

The goals of this research are two-fold, to study effective means of growing ZnSe crystals of good optical quality and to determine the advantages of growing such crystals in microgravity.

Single crystals of zinc selenide have numerous applications in optical devices[1] and consequently there is a demand for crystals of greater optical perfection. They are used as p-n junction light-emitting diodes,[2-6] laser windows, gradient index materials, photo-conductors, etc. When doped with sulfur, the compound ZnS_xSe_{1-x} is a blue emission material. Growth has been achieved under moderate pressure from the melt as well as from chemical and physical vapor deposition, and thin films have been made by evaporation and by epitaxial growth. The growth method used in this study is that of vapor transport and condensation within a sealed quartz ampoule. Physical vapor transport has the advantage of requiring lower temperatures than growth from the melt and it is less vulnerable to the severe strains that can result from growth at very high temperatures. Physical vapor transport is less complex than growth by

chemical vapor transport since the latter method often involves a number of different molecular species, all of whose vapor pressures must be known as a function of temperature.

Boeing Aerospace Company (BAC) and the Consortium for Materials Development in Space (CMDS) expect to fly a joint experiment on the growth of zinc selenide crystals on STS-29, the fourth Shuttle flight after flights resume. In support of the flight system development program, investigators at BAC and UAH are currently concentrating their efforts upon the following four ground-based activities: (1) determination of the optimum growth conditions, (2) growth cartridge development, (3) ground science furnace development, and (4) development of requirements for the flight system. The past year's efforts toward achieving these goals are summarized below.

Crystal Growth

There are four basic steps to crystal growth by physical vapor transport, namely, vaporization of the constituent materials, transport of the vapor to the growth site, condensation of the vapor, and assimilation into the crystal structure. The last of these processes includes the thermally activated movement of adsorbed atoms or molecules about the surface of the crystal. The growth process normally takes place in a thermal gradient such that the condensation zone is 20 to 100°C cooler than the source materials. In a sealed ampoule vapor transport is driven by diffusion and by the difference in partial pressures at the source and the seed, as well as by convection. The actual growth rate is determined by the slowest of the above steps. Experience indicates that step 2, the transport of the vapor to the growth site, is generally the rate-limiting process.

6

In last year's Annual Report it was pointed out that our two major problems were (1) little or no vapor transport and (2) multiple nucleation sites, which, in extreme cases resulted in the formation of a polycrystalline coating on the ampoule wall. The principal factors affecting the vapor transport rate are the thermal profile of the furnace, the stoichiometry and purity of the starting materials, and the residual vapor pressure within the sealed ampoule. Careful pre-treatment of the starting materials is a major factor in enhancing both the stoichiometry and the purity of the materials, with the added benefit of reducing the residual vapor pressure within the ampoule after it is sealed off. Since the furnace had, on a few occasions, produced acceptable transport rates, it was reasonable to assume that the the thermal profile of the furnace was not a major problem. Therefore, it was conjectured that the low transport rates which were frequently obtained were caused by a combination of impurities and poor stoichiometry in the starting material, accompanied by excessively high residual vapor pressures in the ampoules. We then modified our pre-treatment and vacuum bakeout procedures and obtained greatly improved transport rates, as high as 160 mg per day. In the new procedure the ampoule is first cleaned with aqua regia and then rinsed with distilled water, followed by a rinse with methanol or acetone. It is then pumped down to 10^{-6} torr and baked at 1000°C for 2 hours. The ampoule is loaded with 2 to 3 grams of polycrystalline ZnSe obtained from material that had been previously transported. The sample is then refined further by baking at 550°C for two hours under a vacuum of 10^{-6} torr and then sealed off. Using these procedures we achieved the complete transport of all of the starting material in our most recent growth run.

The creation of nucleation sites is the result of the combined effects of the geometry of the ampoule and its cold finger, the position of the ampoule

7

relative to the furnace profile, and the nature of the profile itself. In all early growth runs the transported material formed a polycrystalline cone on the wall of the ampoule at the growth end. Our experimental efforts to obtain single site growth were devoted to modifying the apex region of the ampoule where it joins the cold finger, and to altering the position of the ampoule in the thermal profile of the furnace. Figure 1 shows two stages in achieving better growth. In the upper picture single crystals of millimeter size emerge from the polycrystalline layer on the ampoule wall. In the lower picture there is no polycrystalline layer; instead, single crystals of millimeter size grew at discrete sites on the ampoule wall. Best results were obtained by extending the ampoule into a narrow tube in the cold finger as shown in Figures 3 and 4. Using this method several boules containing single crystals of nearly centimeter size were obtained without any material sticking to the ampoule walls. Photographs of these large crystals are shown in Figure 5.

As of this date the optimum conditions for crystal growth have not been determined. However, successful growth runs were made in both of the furnaces shown in Figures 2 and 3. Figure 2 shows the temperature profile for a Marshall furnace operating at a source temperature of 1000°C and a growth temperature of 975°C. A transport rate of 145 mg/day was obtained during a 10-day run. Figure 3 shows the profile for the single-zone BAC #0 furnace. With a source temperature of about 940°C and a temperature difference of about 60°C, a transport rate of 168 mg/day was obtained during a 15-day run. Five successful growth runs have been completed as shown in Table I. Four of these runs have produced the crystals shown in Figure 5. Four boules weighing 1.4 to 3 grams have been obtained to date. Each of these boules contains a relatively large

8

TABLE I

BOULE NUMBER	WEIGHT (Grams)	SOURCE/GROWTH TEMP (oC)	RUN TIME (DAYS)	AV.GROWTH RATE mg/day	FURNACE	TRANSPORT
2	1.44	1003/976	10	144	Marshall	Incomplete
3	2.52	940/880	15	168	Transparent	Incomplete
4	2.04	1003/976	20	102	Marshall	Incomplete
5	0.5	1003/976	22		Marshall	Incomplete
6	3	1003/976	32	100	Marshall	Complete

single crystal, although the boule as a whole is a composite of many crystallites. Three of these boules are shown in Figure 5.

Crystal Characterization

Crystals will be characterized during the next year by means of the following methods. First, they will be examined for their structural and compositional purity using x-ray diffraction, optical and electron microscopy and Raman spectroscopy. Secondly, they will be evaluated for applications in optical devices by such measurements as optical absorption, luminescence, photoconductivity, and the Hall effect.

Growth Cartridge Development

BAC has gained approval for the basic cartridge design as shown in Figure 6. It involves the use of two-walled ampoules which provide two levels of containment of the sample materials. BAC will evaluate the cartridge for mechanical strength and for its ability to provide the appropriate thermal environment within the prototype flight furnace. UAH will study crystal growth in the two-walled cartridge using the BAC #1 furnace.

Ground Science Furnace Development

UAH and BAC are working together to improve the ground science furnace. Later this year BAC will build and deliver a rotatable test stand so that convection studies can be carried out. BAC will also provide a programmable ampoule drive mechanism and a multizone heater system to facilitate future studies.

Presentations and Publications

1. Jason M. Kinser, Growth of Zinc Selenide Crystals by an Open Ampoule Method, Masters Thesis, The University of Alabama in Huntsville, 1987.

2. Jason M. Kinser, Elmer E. Anderson and M. K. Wu, "Growth of Zinc Selenide by Vapor Transport in an Open Ampoule," Bull. Amer. Phys. Soc. 32, 610 (1987). Paper presented at the NY APS Meeting, March 1987.

3. Jason M. Kinser, "Growth of ZnSe by Vapor Transport in an Open Ampoule." Paper presented at the March 1987 meeting of the Alabama Academy of Sciences, Florence, Alabama.

4. Hai-Yuin Cheng, Elmer E. Anderson and M. K. Wu, "Growth of ZnSe by Physical Vapor Transport," Bull. Amer. Phys. Soc. 32, 610 (1987). Paper presented at the NY APS meeting, March 1987.

References

1. Oliver, D. S. and W. R. Buchan, IEEE Trans. Electron Devices ED-18, 769 (1971).

2. Allen, J. W., A. W. Livingstone and K. Turvey, Solid State Electron. 15, 1363
                         (1972).
3. Ozsan, M. E. and J. Woods, Appl. Phys. Letters 25, 489 (1974).

4. Ozsan, M. E. and J. Woods, Solid State Electron. 18, 519 (1975).

5. Ozsan, M. E. and J. Woods, J. Phys. D 10, 1335 (1977).

6. Lawther, C. and J. Woods, phys. stat. solidi 50a, 491 (1978).

Figure 1. Small crystals of ZnSe. Magnification:
upper photo x 48, lower photo x 10.

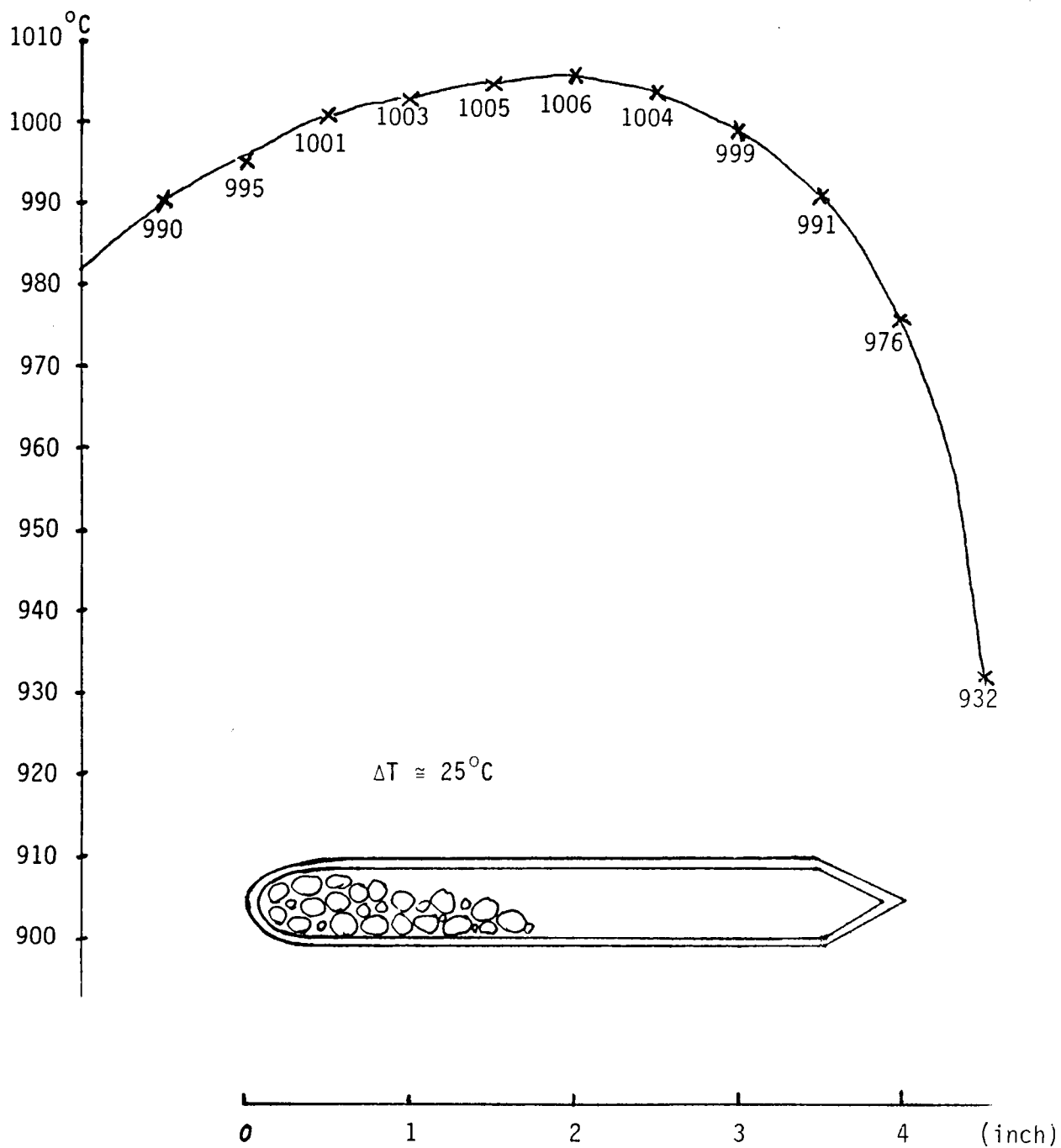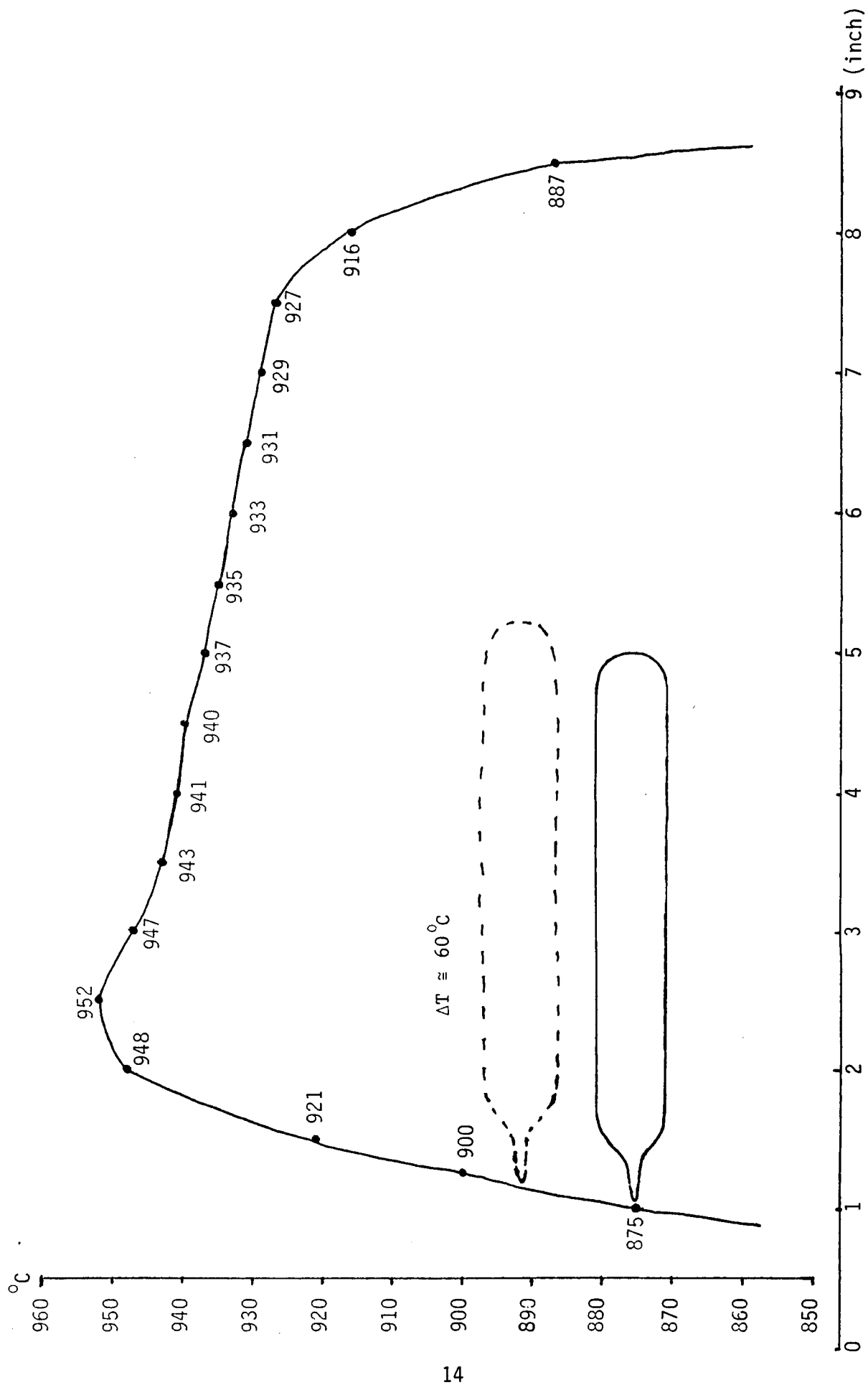Fig. 2. Marshall Furnace Temperature Profile and Growth Position

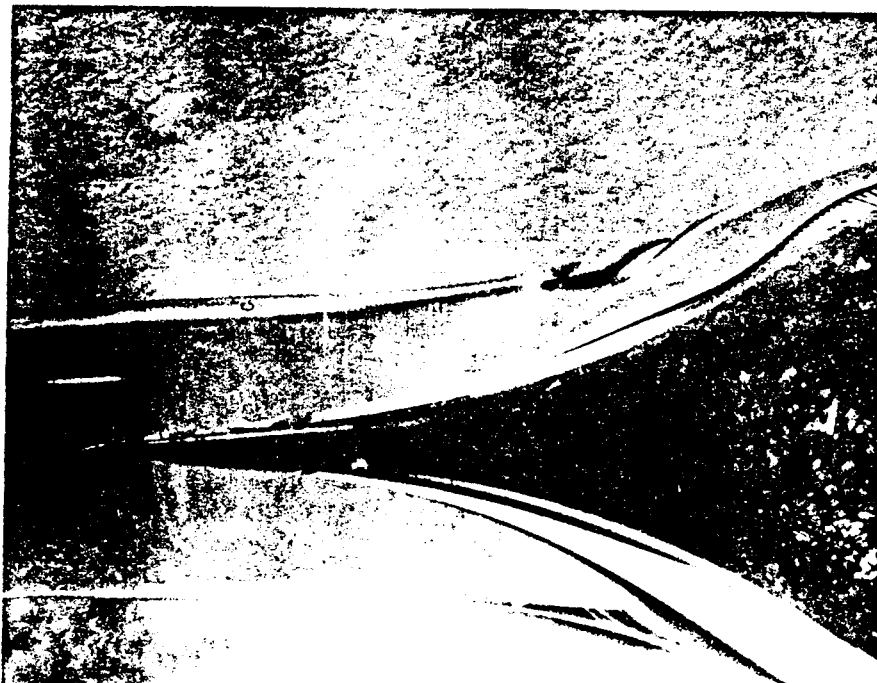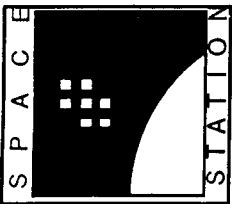Fig. 3. Boeing #0 Furnace Temperature Profile and Growth Position

14

Fig. 4. Growth channel in the cold finger.
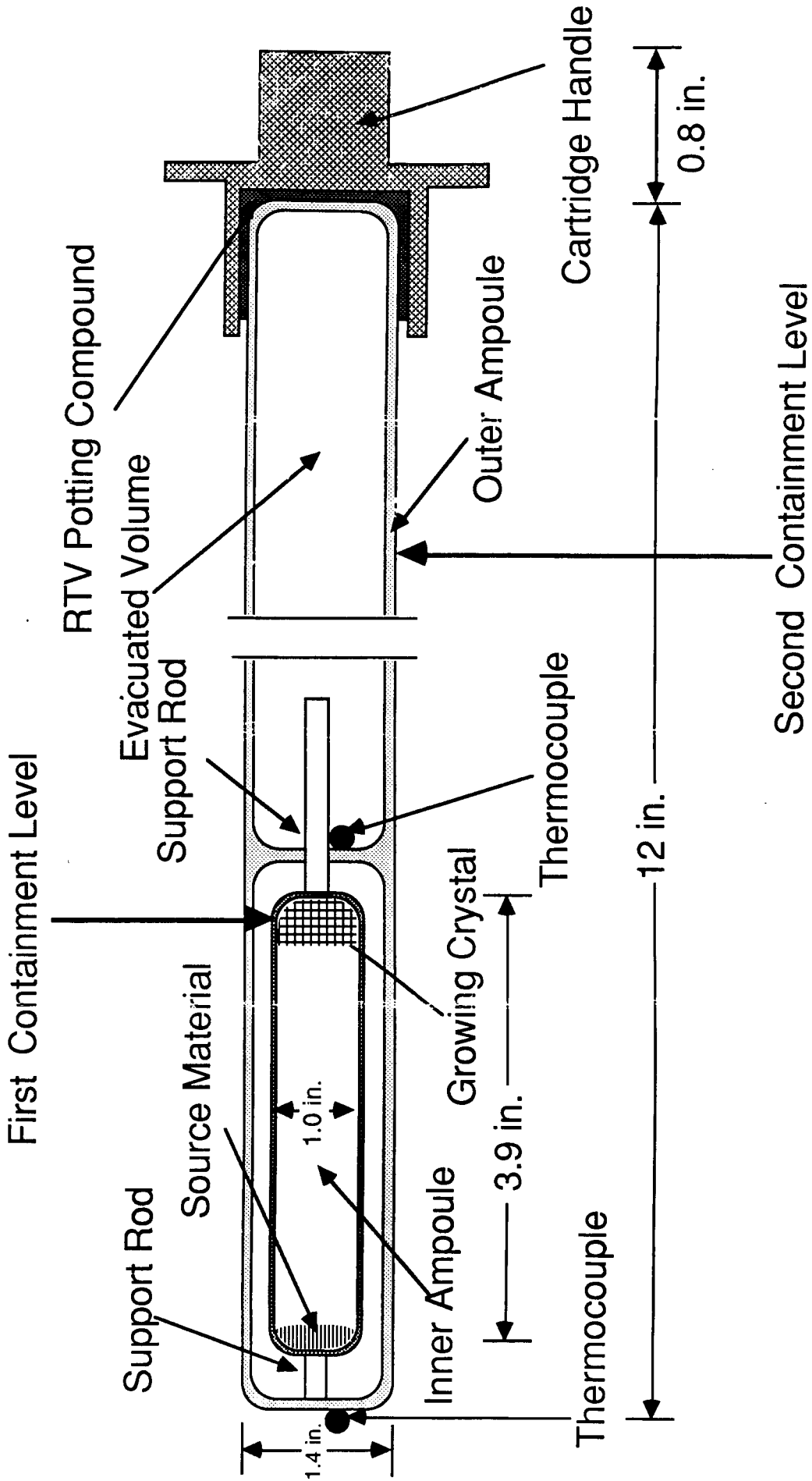Magnification: x 6.3.

Fig. 6. Boeing Cartridge Baseline Design

Center: Consortium for Materials Development in Space
         The University of Alabama in Hunstville (UAH)

Project Name: **Physical Vapor Transport Crystal Growth**

Subproject Name: **Mass Spectroscopic Facility**

The University of Alabama in Huntsville
                          Franz Rosenberger

Annual Report: September 15, 1986 to September 14, 1987

* *

Introduction

Both the Consortium for Materials Development in Space and the Center for
Microgravity and Materials Research (CMMR) are pursuing projects that will
greatly benefit from an inhouse chemical characterization of materials at high
temperatures. Since CMMR personnel has experience with the mass spectroscopy of
high temperature vapors, it was decided to establish a joint mass spectroscopic
facility.

A mass spectrometer system was designed consisting of:

- Balzers QMG 511 Quadruple Mass Spectrometer (mass range 2-1023, cross
  beam ion source with electron acceleration voltage adjustable 5-120V)

- Balzers TSU 170 Turbomolecular Pump Station (170 1/sec)

- Alcatel 37-63M/E2M2G Diffusion Pumping System (for evacuation of (dirty)
  sample furnace space)

- Various high vacuum gauges and liquid nitrogen traps

- Teknivent Vector/One Mass Spectrometer Computer for control and data
  acquisition.

The acquisition of these components has been completed.

The remaining tasks for the completion of the mass spectroscopic facility

consist of the design and construction of a:

- a vapor inlet system with cryogenic collimator, that minimizes the forma-
  tion of molecular species that are sample-non-specific;

- a cryogenic chopper for the molecular beam, that in connection with phase-
  locked signal acquisition will increase the signal-to-noise ratio; and

- a multi-zone, programmable sample furnace.

These parts of the system are being designed and will partly be constructed in
the UAH metal shop. Complete assembly and first test runs with the whole system
can be expected in 8-9 months.

The first investigations to be conducted with the completed facility will be
concerned with the high-temperature out-gassing behavior of quartz ampoules and
the vapor composition in crystal growth experiments of the CMDS. These will
give important insight on the prevailing transport mechanisms in these crystal
growth experiments and supply a realistic basis for the numerical modeling of
heat and mass transfer in these systems.

Center: Consortium for Materials Development in Space
          The University of Alabama in Huntsville (UAH)

Project Name: "Materials Preparation and Longevity in Hyperthermal Atomic Oxygen"

Industrial Participant: Martin Marietta Denver Aerospace
                          Box 179/Mail Stop M-0487
                          Denver, CO 80201
                          Lyle E. Bareiss
                          Gary P. Sjolander

The University of Alabama in Huntsville
          John C. Gregory

Annual Report: September 15, 1986 to September 14, 1987

* *

Introduction

This report includes work on the following tasks:

* Flight Hardware Fabrication

    EOIM-3

* Design and Fabrication of Atom Beam Source

* Construction of Surface Science Laboratory

* Progress in research on processes and mechanisms of interaction of

    hyperthermal atoms at solid surfaces.

* Publications since October 1986

Preparation of Flight Hardware

EOIM-3

Substrates: LiF and graphite single crystals have been purchased. Vitreous

carbon discs were cut and polished during the previous quarter and preparation

of additional samples continues. These surfaces will shortly be characterized

using stylus profilometry and polarizing microscopy.

Silver Detectors: Fifteen CR-39 detector strips were purchased, cut to fit the UAH Scatterometers and coated with Ag using the MSFC RF sputtering facility. These surfaces will shortly be characterized using scanning microdensitometry.

Thermal Atom Beam Facility

The thermal energy oxygen atom beam facility is designed to complement, not duplicate, the much more expensive 5eV atom beams under development at MMDA and elsewhere. It will provide a quantitative basis of comparison with data from these other more energetic sources and from space. The use of discharge "ashers" as oxygen atom sources is quite inadequate for quantitative research necessary to understand the basic reaction mechanisms. The system is designed to provide a known flux of oxygen atoms in the range $10^{14} - 10^{15}$ atoms/cm^2/sec to a target surface maintained in vacua in the 10^{-7} torr range. Using proven designs allows us to have a usable beam at the lowest possible development cost. The design was based on concepts used in several laboratories, including Aerospace Corporation[1] (see also ref. 2 and 3).

The facility is presently under construction. The two major elements of the three-chambered differentially pumped molecular beam apparatus (which may be later adapted to a four-chamber design) consist of a microwave discharge source for the production of an intense beam of atomic oxygen, and a target chamber for reaction studies and beam characterization.

Figure 1 shows a schematic representation of the molecular beam apparatus. The three chambers will be differentially pumped by turbomolecular, ion and cryogenic pumps respectively. Due to the pumping capacity of the turbomolecular pump in the source chamber (chamber 1) sufficient removal of molecular oxygen should occur such that a cryogenic pump can be safely assigned to the sample

Figure 1.

ATOMIC OXYGEN FACILITY
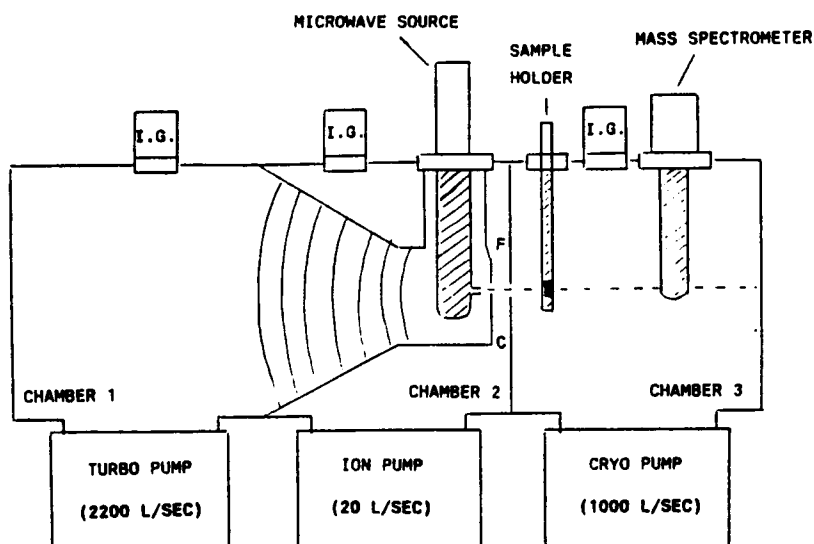
C: POSITION FOR CHOPPER

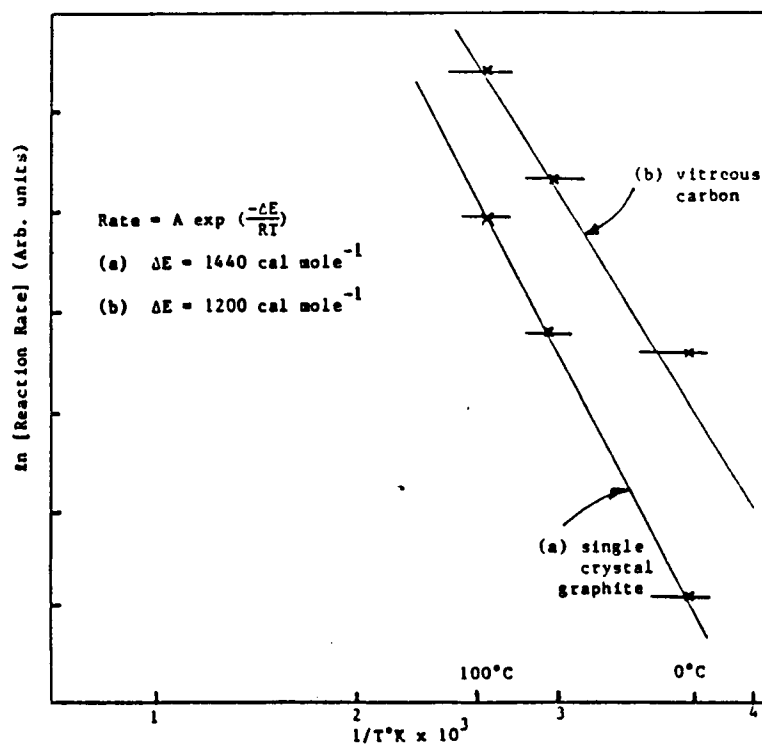F: POSITION FOR FLAG

I.G.: IONIZATION GAUGE

Figure 2. Arrhenius Plots for Carbon Oxidation by 5eV Oxygen Atoms (STS-8 data)

chamber (chamber 3). Chamber 2 acts as a collimating chamber, and will also contain beam chopping and flag facilities for the characterization of beams produced. Figure 1 shows the extent to which chamber 1 will be extended into chamber 2. This is to ensure the smallest separation between the microwave discharge source exit orifice and the sample to be exposed, to minimize beam divergence effects. This separation will be approximately 6-8 inches.

The vacuum system is to be based on a 12" diameter stainless steel tubing design, with internal divisions to separate individual chambers. Materials are currently being purchased. Appendage pumping and other chamber accessories are awaiting delivery.

A substantial part of the microwave discharge source has been constructed, the predominant material used being brass. Oxygen atoms will be produced by inducing a microwave discharge in a gas mixture containing O_2. The beam source employs a cavity very similar to that described by Murphy and Brophy.[2] The cavity is a $3\frac{1}{4}$ wave foreshortened coaxial type, with microwave power coupling and cavity tuning of the Evenson design.[3] Power will be supplied to the cavity by a Raytheon PGM-10 2450-MHz magnetron power supply. The discharge tube is of fused silica, 6 mm in diameter with an exit orifice diameter of 1.0 mm.

Progress in Construction of the Surface Characterization Laboratory

Although not funded under the CMDS project, the surface characterization equipment to be installed in this facility is central to the surface research planned for the Consortium year 1987/88. A Perkin-Elmer PH1-5400 small-spot x-ray photoelectron spectrometer has been delivered and a Kratos X-SAM-800 Scanning Auger Spectrometer has been ordered. Contracts for renovation of the building space are well under way. We expect to have our first XPS spectra of surfaces exposed to atomic oxygen soon.

23

Progress in Research on Processes and Mechanisms of Interaction of Hyperthermal
Atoms at Surfaces

We have previously described our experiment on the STS-8 mission on which
the first kinetic data and scattering studies of 5eV O atoms were obtained.

The conclusions form the measurements on various forms of carbon exposed in
the STS-8 mission appear applicable to organic solids in general. They may be
summarized as follows:

1. Measured erosion was linear with total fluence.

2. No induction time was observed before onset of erosion.

3. Erosion rate linear with oxygen flux (i.e., reaction probability inde-
    pendent of flux) measured over a small range, 1.5 to 2.5 x 10^{15} atoms
    $cm^{-2}s^{-1}$.

Our experiments used very pure materials, but standard or engineering mate-
rials may be contaminated either on the surface or by inclusions in the bulk.
Such contamination, if less oxidizable than the matrix itself, may then serve to
protect the rest of the matrix material from erosion. As erosion proceeds the
density of these screening particles or films on the surface grows and the
erosion rate may drop from its prior value. Such protection may result in
erosion measurements and derived rates considerably less than those for pure or
unprotected material. We have shown that thin films of silicone deposited in
space were converted to a layer of SiO_2 2 to 3 nm thick by the ambient oxygen
atoms. This film, which overlaid a carbon surface, provided protection from
attack by oxygen atoms.

The temperature-dependent rate data for CR-39 were as follows:

Temperature °C	0-20	65	115
Erosion (nm)	22,600	25,000	29,000

24

Similar data were obtained for the other substrates. Arrhenius activation energies (see figure 2) for some of these were calculated to be:

Material	E (cal mol^{-1})
CR-39	650
vitreous carbon	1200
graphite (basal plane)	1400

These values are quite consistent with literature values of activation energies of $O(^3P)$ with some organic compounds in the gas phase.

While reaction probabilities for carbon surfaces may be simply expressed in terms of C atoms lost per incident O atom (we have measured such probabilities with 5eV oxygen in the range 0.1 to 0.15 atoms per atom), for more complex substrates, reaction probabilities have been expressed in cm^3 x 10^{-24} of material lost per incident O atom. Probabilities for some polymer films were summarized by Leger et al.[4]

Typical values were, at about 300°K (in the units cm^3) x (10^{-24} atom^{-1}) as follows:

CR-39 $(C_{12}H_{18}O_7)_n$ (this work)	6.0
Kapton (an aromatic imide) (ref. 4)	3.0
PMMA (this work)	4.8

Discussion

Comprehensive reviews of atomic oxygen reactions with organic compounds are available.[7,8] It is now well established that the first step of the reaction of $O(^3P)$ with alkanes is abstraction of hydrogen:

$$RH + O \longrightarrow R\cdot + OH$$
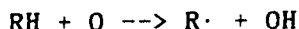
though other possibilities may still occur. In the case of second and further interactions of the same residue with oxygen atoms, however, the picture is very complex and obscure. For the case of surfaces of solid polymers under consideration here, subsequent addition reactions almost certainly occur, but after each addition or abstraction the possibility exists for rearrangement and loss of a volatile fragment.

Reactions with halo alkanes proceed via abstraction of available hydrogen since abstraction of halogen is too endothermic, at least in the case of thermal energy O(3P). This may not be the case for 5eV oxygen atoms, though polyfluorinated hydrocarbons are clearly less reactive in the space environment. Reaction with completely halogenated hydrocarbons may also proceed by addition mechanisms[9], which may be facilitated by a kinetic energy of 5eV. The massive erosion of fluorinated polyethylene observed on materials returned from the solar maximum repair mission was a surprise. The result has been interpreted in terms of the hydrogenated fraction of the material. The reaction rate of fully fluorinated polymers with 5eV oxygen atoms remains unquantified.

For alkenes and alkynes O(3P) adds to the unsaturated bond forming either stable products or rearranging and fragmenting. The relative frequency of these processes depends on the ability of the molecule to accommodate the excess energy according to Cvetanovic[10]. This ability is high in the case of surface reactions, but the behavior with 5eV atoms is quite uninvestigated.

Reactions of O(3P) with aromatic compounds is the least well understood. Oxygen atoms may add to a carbon atom in benzene forming a radical which may rearrange to give phenol:

$$O\cdot \ +\ \text{(benzene)} \longrightarrow \left[\text{(cyclohexadienyl-O·H complex)} \right]^{*} \longrightarrow \text{(phenol)}\ OH$$
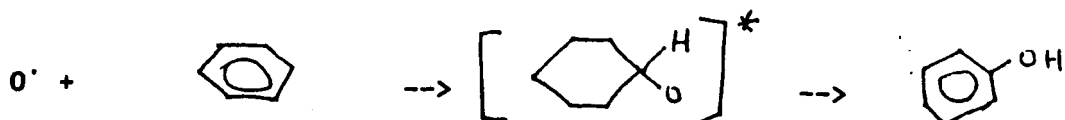
    If a free radical remains in the surface after the first atom reaction, then reaction may occur with another atom. Since the atom-arrival rate of oxygen atoms in low earth orbit is about 1 per surface atom per second, the radical lifetime must be at least this long. Laboratory data on atom-radical reactions is sparse with a considerable amount of data available only for methyl radical reactions. There is however much published information on decomposition path-ways of radicals, including those containing oxygen, and these allow deductions to be made on probable reaction paths.

    $O\cdot \ +\ R\cdot \ \longrightarrow \ [RO\cdot]^{*} \longrightarrow$ products

As Huie and Herron point out, however, even in the case of thermal $O(^3P)$ the produced radicals are most probably excited and other pathways become energetically possible.

    The situation is further complicated in the present case if 5eV kinetic energy is available (though this may not be the case; see conclusion below). Also there is a greatly increased possibility of de-excitation of various species at the solid surface. Thus, although a good deal of data exists on reaction path ways of free-radicals with oxygen atoms, the number of possibilities for reaction with polymeric surfaces is so large that elucidation of actual reaction pathways needs experimental measurement in situ of chemical species present on the surface and mass spectrometric measurement of product composition and energy.

    A number of general conclusions can be drawn from the extensive literature on rates of reaction with $O(^3P)$. Some of these are:

- The attack of $O(^3P)$ on carbon compounds is electrophilic in nature.
- For alkanes, secondary hydrogen atoms are 10 to 20 times more likely to be abstracted than primary hydrogen atoms.
- Results for $O(^3P)$ reactions with substituted benzenes shows this electrophilic nature, rate constants varying 2 orders of magnitude from $C_6H_3(CH_3)_3$ to C_6H_5F and $C_6H_5CF_3$.

These conclusions are modified in the case of $O(^1D)$ reactions and may also not be valid with 5eV $O(^3P)$.

Conclusions

Activation energies have been measured for 5eV $O(^3P)$ reactions with solid polymer and carbon surfaces in orbit in the range 4-7 kJ mole^{-1}. These are similar in magnitude to those observed in a variety of reactions of thermal $O(^3P)$ with organic compounds. This fact would be consistent with a model in which the rate-controlling step in the reactions of 5eV oxygen atoms with solid organic surfaces actually involved thermalized O atoms bound at the surface, perhaps in a mobile precursor state. This is also consistent with a measurement of the angular distribution of 5eV oxygen atoms scattered from a carbon surface[11], which showed almost (but not quite) complete energy accommodation. The present authors have also shown, however, that the absolute rate of the reaction of 5eV atoms with carbon surfaces is several times that of thermal atoms. This dependency of rate on kinetic energy only applied, according to this model, to the adsorption step of oxygen into the precursor state. The actual reaction with the organic moiety in the surface to form products may not need to consider the inclusion of 5eV of excitation energy that has already been dissipated. The following reaction sequence is postulated:

activated adsorption	O (fast) $+ S \longrightarrow O_S^*$
dexcitation	$O_S^* + S \longrightarrow O_S + S$
re-emission	$O_S \longrightarrow O_g$
reaction	$O_S + RH \longrightarrow [RHO]^*$
	$[RHO]^* \longrightarrow$ products

This conclusion means that the extensive data on thermal $O(^3P)$ reactions may be useful (in so far as gas-phase reactions may be correlated with surface reactions) in interpreting surface reactions of $O(^3P)$ at 5eV.

It should be noted that this does not apply to gas-phase reactions of oxygen atoms with molecules surrounding the Shuttle Orbiter which have been postulated to give rise to the extended Shuttle glow[12]. In this case, intermediates and products will be produced in high energy electronic and vibrational states.

In the final quarter several samples from the space flight STS-8 were analyzed in the newly commissioned UAH x-ray photoelectron spectrometer. Materials investigated were copper, iridium and polymethyl methacrylate. This work is continuing and will be disc   ed in the next quarterly report.

REFERENCES

1. Arnold, G. S. and D. R. Peplinski, <u>Proc. 13th Space Simulation Conf.</u>, NASA CP-2340, Oct. 1984, p. 150.

2. Murphy, E. J. and J. H. Brophy, <u>Rev. Sci. Instrum. 50</u>, 635, (1979).

3. Fehsenfeld, F. C., K. N. Evenson and H. P. Broida, <u>Rev. Sci. Instrum. 36</u>, 294, (1965).

4. Leger, L. J., J. T. Visentine and J. F. Kuminecz, AIAA Paper No. 84-9548, January 1984.

5. Whitaker, A. F. <u>et al</u>, AIAA paper 85-0415, (1985).

6. Hansen,R. H., J. V. Pascale,T. Benedictis, and P. M. Renzepis, <u>J. Polymer Sci:PtA</u>, <u>3</u>, 2205, (1965), 183, (1984).

7. Cvetanovic and Singleton, <u>Rev. of Chem. Intermed. 5</u>, 183, (1984).

8. Huie, R. E. and J. H. Herron, <u>Prog. React. Kin. 8</u>, <u>(1)</u>, p. 1-80, (1975).

9. Ung, A. Y-M. and H. I. Schiff, <u>Can. J. Chem. 40</u>, 486, (1962).

10. Cvetanovic, R. J., <u>Advan. Photochem. 1</u>, 115, (1963).

11. Gregory, J. C. and P. N. Peters, <u>Rarefied Gas Dynamics 15</u>, (1986).

12. Gregory, J. C. and P. N. Peters, <u>Second Workshop on Spacecraft Glow</u>, NASA CP-2391, p. 174, (1985).

Publications (Since October 1986)

    a. Journal Articles and Published Proceedings

1. "A Measurement of the Angular Distribution of 5eV Atomic Oxygen Scattered off a Solid Surface in Earth Orbit", J. C. Gregory and P. N. Peters, Rarefied Gas Dynamics 15, 644, (1986).

2. "Free Molecule Lift and Drag Deduced from Shuttle Flight Experiment", G. R. Karr, J. C. Gregory and P. N. Peters, Rarefied Gas Dynamics 15, 604, (1986).

3. "Reaction of 5eV Oxygen Atoms with Polymeric and Carbon Surfaces in Earth Orbit", J. C. Gregory and P. N. Peters, Polymer Preprints, accepted for publication, April (1987).

4. "Interaction of Hyperthermal Atoms on Surfaces in Orbit: The University of Alabama Experiment", J. C. Gregory, invited paper in Proc. of the NASA Workshop on Atomic Oxygen Effects, Jet Propulsion Laboratory, Pasadena CA, Nov. 10-12, (1986).

5. "Oxygen Atom Velocity Distributions as Viewed from a Spacecraft and Their Use to Determine Thermospheric Temperatures", P. N. Peters, R. C. Sisk and J. C. Gregory, Journal of Spacecraft and Rockets, (1987), accepted for publication, November (1986).

    b. Presentations

1. NASA Workshop on Atomic Oxygen Effects, JPL Pasadena, Nov 10-12, 1986.

2. American Chemical Society Annual Meeting, August-September 1987, New Orleans.

3. European Conference on Application of Surface and Interface Analysis, Stuttgart, October 1987 (Two abstracts submitted.).

Center: Consortium for Materials Development in Space
         The University of Alabama in Huntsville (UAH)

Project Name: **"Surface Coatings and Catalyst Production by Electrodeposition"**

Industrial Participant: McDonnell Douglas Astronautics Company - Huntsville
                         Chester B. May

The University of Alabama in Huntsville
                         Clyde Riley
                         H. Dwain Coble
                         Boon H. Loo

Annual Report: September 15, 1986 to September 14, 1987

* *

Introduction

This project involves study of electrodeposition and electrocodeposition in low g, and applications of this process. During the course of our investigations we hope to provide a better understanding of (a) the role of convection and buoyancy in the mechanisms for formation of some electrodeposited surfaces, (b) fluid flow in the vicinity of electrodepositing surfaces, (c) the influence of (lack of) a moving medium upon codeposition, (d) the effect of gravity upon the dispersion (coagulation) of neutral particles that are desired for codeposition and (e) preparation of improved surface coatings and metal catalysts. As pointed out previously there is evidence for peculiarities during low g electrodeposition of at least two of the systems we have chosen for investigation.[1] Whether for purely scientific or applications reasons these particular systems require further study.

Background

1. Simple Electrodeposition

We consider the reduction of a metallic cation in aqueous solution at the cathode:

$$M^{n+}(aq) + ne^- \rightarrow M(s) \tag{1}$$

where e^- denotes an electron and $M(s)$ represents metal atoms depositing on the cathode. Assuming one dimensional flow, the concentration of ions in the vicinity of a diffusion controlled electrode may be found by solving Fick's second law

$$\frac{dC(x,t)}{dt} = D\frac{d^2C}{dx^2} \tag{2}$$

This represents the time variation of cation concentration C in a plane parallel to the electrode at a distance x, where D is the diffusion coefficient for the cation. For constant current/flux conditions the solution of (2) becomes[2]

$$C(x,t) = C_0 - \frac{2It_-}{nF}\sqrt{\frac{t}{D}}\ \text{ierfc}\ \frac{x}{2\sqrt{Dt}} \tag{3}$$

where I is the cell current, t_- is the anion transport number, t is the time, F is the Faraday constant and ierfc is the integrated error function. A well behaved diffusion controlled electrode system should produce a concentration which behaves as (3).[3] Equation (2) can also be utilized to evaluate the instantaneous current[4,5]:

$$i_t = \frac{nFAD^{1/2}C_0}{\pi^{1/2}t^{1/2}} \tag{4}$$

where A is the area of the electrode and C_0 is the initial or bulk concentration of the cation in the cell. Equation (4) represents the instantaneous current at an electrode under diffusion control as a function of time.

2. Codeposition

The latest theoretical treatment of electrocodeposition was formulated in 1972 by Guglielmi.[6] He applies a modified Langmuir adsorption isotherm utilizing a two step process for occlusion of the neutrals (cermets) within the forming metal matrix. Particles are initially loosely adsorbed on the surface and are treated as being in equilibrium with those in suspension. Guglielmi's treatment assumes homogeneous suspension and ionic concentrations of Cm and Co respectively. This results in a working equation given by [6]

$$\frac{Cm}{\alpha} = \frac{Wi_o}{nFd\nu_o} e(A-B)\eta \left[\frac{1}{k} + C_m\right] \tag{5}$$

where α is the volume fraction of particles in the deposit, W is the atomic weight of the depositing metal, F Faraday's constant, n the number of electrons required to reduce the cation to an atom, d the metal density, $\nu oeB\eta$ is an exponential rate factor for strong adsorption in which η is the overpotential and ν_o, A and B are adjustable parameters, i_o is the exchange current, and k is the ratio of rate constants for adsorption and desorption which depends upon the intensity of interaction of the particles and the electrode. If the system is not homogeneously maintained as would be the case in low g without stirring, the suspended particles and solution ions would form gradients and thus equation (5) is not applicable.

Experimental Work

1. General

The eight cell flight apparatus (Model I) has been completed and is pictured in Figure 1. It has been partially tested for short 10^{-2} g periods on the

34

KC-135. The stirrers, camera and electrodeposition systems were tested during these flights. The meter systems for measuring current, voltage and temperature, and the computer interface board were not utilized. Batteries with dividers were used for power. Data was gathered on particle dispersion during stirring in 10^{-2} g, and Ni and Co surfaces were generated at 10^{-2} g in multiples of $\simeq 20$ second increments. Electrodeposition rates were altered by changing the applied voltage. It was found that the apparatus was cumbersome for the KC-135 experiments which are more amenable to operator interaction and fast turnaround times. So although the apparatus functioned as designed during these limited tests, two smaller and simpler packages were constructed to maximize future KC-135 testing. These packages are pictured in Figure 2. Cells could now be "plugged" into position and the voltage divider approach allowed four different rates of electrodeposition simultaneously.

2. Bench Testing

a) Simple Electrodeposition

Work was done on a Sn/Ni alloy cell. A composite solution of ~65% Sn, 35% Ni is reported to produce a nice alloy plating of SnNi (1:1) composition.[7] We wanted to look for differences between bench and low g electrodeposited alloys. Thus far the cell has produced dendritic crystals (much like most silver solutions) instead of smooth plates. Hopefully we will solve this problem so we can run this system on the KC-135.

The $CoSO_4$ cell as previously reported was found to self terminate after 2 hours on the bench when operated in a cathode over anode diffusion mode.[1] Hand agitation of the cell for several minutes and

35

subsequent restart lead to oscillatory behavior. Since our evidence showed that diffusion controlled CoSO4 • 7H2O crystallization at the anode was responsible for this peculiar behavior an internal stirring bar was placed in the cell. When the cell terminated after about 2 hours it was agitated magnetically. With the homogeneity of the solution now renewed upon restart the cell functioned as a new cell, running for about 2 hours before self termination.

b) Polystyrene Neutral Buoyancy Codeposition

This work has been frustrating but yet rewarding in terms of how to prepare for low g codeposition. As pointed out previously this attempt at physical modeling of low g codeposition has a major flaw.[1] As the electrodeposition progresses under diffusion control a concentration gradient and thus a density gradient is developing. On the bench this results in settling or layering of the particles due to the solution/particle density mismatch. The resultant settling would not occur in low g. However, another difficulty will result during diffusion control in low g, namely a neutral particle gradient. Since these particles are micron size, Brownian motion will be slow (small diffusion constants) and it is expected that particle deposition will decrease rapidly with time producing a particle gradient in the codeposited surface.

c) K1•75Pt(CN)4 • 1.5 H2O Crystallization

The senior undergraduate is concentrating on cell development and construction. He has obtained $4,000 from Westinghouse to help support the project.

Results and Conclusions

1. Oscillatory Cell

Utilization of a stirring bar in the cell allowed us to return the solution to its initial concentration homogeneously throughout the cell cavity and thus no oscillatory process resulted upon restart after stirring. Apparently hand agitation only changes the anode $CoSO_4 \cdot 7H_2O$ coating and Co^{+2}, SO_4^{-2} gradients enough to bring on the oscillatory behavior.

2. Codeposition

One of our goals on the first KC-135 flight was to determine what happens when particles like Cr_3C_2 and diamond dust are dispersed by a stirrer in liquid. On our first flight we used 1 M $ZnSO_4$ as the medium in the top two stirred cells of our planned space flight apparatus (Figure 1). Dispersion of the particles was monitored with a 35 mm camera. It was interesting to find that Cr_3C_2 particles tended to coagulate into spherical balls when the stirrer was activated in low g (Figure 3). Evidence as to the effect of the addition of wetting agents on this particular flight was not obtained because the film was lost. We could not tell from the other photographs whether the diamond dust was coagulating or not. On the second KC-135 flight we used a different codeposition apparatus which was monitored with a video recorder. It was evident from the videos that both Cr_3C_2 and diamond dust clump when stirred at 10^{-2} g. Addition of cationic, cetyltrimethylammonium bromide surfactant had little effect. However, addition of anionic sodium dodecylsulfate resulted in good dispersion of the Cr_3C_2. We found no evidence for coagulation of these particles when stirred in 1 g.

Scientifically this is interesting since we may have evidence for a weak force process that is swamped by 1 g. Zeta potential measurements would probably be helpful in determining why an anion agent is necessary for dispersion of Cr_3C_2. From an applications standpoint homogeneous dispersion is necessary if we are to optimize the electrocodeposition process and our findings indicate we would have to determine if the particles were going to disperse anytime we changed particle type or solutions and if not what surfactant (if any) would aid in the dispersion.

As mentioned previously, a particle gradient will be created as the codeposition procedes in low g. It would seem that advantages of a low g codeposition would arise from no natural convection, particle sedimention or solvent movement which should lead to more homogeneous and richer codeposits. However, the particle gradient results in a time decrease in the volume fraction of particles in the forming surface. To obviate this problem would require some form of stirring and we must determine if the stirring should be a gentle slow continuous stirring with a disk as done by Ehrhardt[8] or a sequence consisting of an intermittent fast stirring followed by a damping period of non electrodeposition, and finally a short period of electrodeposition of say 10 minutes. This sequence would then be repeated for 6 hours of total electrocodeposition.

3. Catalyst Preparation

One of our goals is to use low g to electrodeposit metals in forms that may improve their function as catalysts. Ehrhardt[8] argues that an amorphous form of nickel results when nickel is deposited relatively fast in low g at 6 volts and a current of 80 mA/cm^{2}. Since amorphous metals tend to resist acid attack, amorphous Ni may be a candidate for an improved catalyst under acid conditions.

Likewise, if amorphous Ni is being produced, is it due to low g, fast rate, fast rate plus low g or what? We ran samples in the laboratory at 1.5, 3.0, 4.5 and 6.0 volts in the cathode over anode diffusion mode and in the anode over cathode convection mode. We accumulated ~3-5 minutes of repetitive 20 second runs on the KC-135 also at 1.5, 3.0, 4.5 and 6.0 volts. Comparisons were made of the surface x-ray diffraction patterns with those on the bench. Patterns for nickel fcc crystalline planes were identified in all cases. To determine what an amorphous Ni x-ray pattern looked like an Ni-P amorphous alloy was prepared by a chemical technique.[9] Its x-ray pattern was typical of a nearest neighbor amorphous material consisting of only one broad peak. Comparison was also made with a hypothetical scan of pure amorphous Ni (prepared by a cold splat technique) transposed from an electron diffraction pattern which showed three broad nearest neighbor peaks.[10] No such pattern existed in our data, only crystalline planes associated with a Ni fcc structure. Our strict interpretation of x-ray data, presented by Ehrhardt[8] to demonstrate amorphous Ni electrodeposition, showed evidence for crystalline planes and not a typical nearest neighbor amorphous pattern. However, their data could be loosely interpreted as representing a mixture of amorphous and crystalline Ni since their x-ray peaks corresponding to various Ni crystalline planes were small. On the second KC-135 flight we accumulated Ni at rates associated with up to 12 volts. The x-ray data although not complete is not encouraging since there is still no evidence for broad nearest neighbor peaks. Low g plates of Pd and Co were also accumulated by the same repetitive technique. Co was done at a relatively fast rate for two pH's ~ 1.9 and 4.5. Incomplete x-ray data of the cobalt gives indications of a peculiarity which we have not interpreted yet.

Immediate Future Planned Work

We shall work on producing surfaces on the KC-135 and look for peculiarities or differences relative to that of a bench diffusion mode. We are assembling diode array spectrometer to study ion concentration gradients in the vicinity of an electrode on the KC-135 by a wavelength specific adsorption technique.[11] We will work with a $CuSO_4$ system first since it should work well with an He-Ne laser. We will follow this with a study of the $CoSO_4$ system for which there is evidence of a difference in the concentration gradient between the 1 g diffusion mode and the KC-135 data.[4,12] Both the low g and 1 g data will be accumulated on the KC-135. A solution light path of 2-3 mm will be utilized to minimize light deflection errors.[13,14] Comparison with equation (3) should then be possible. Figure 4 demonstrates schematically our planned arrangement.

Late Developments

Data has been analyzed from the June and August KC-135 flights.

1. Stirring/Codeposition

In the August KC-135 flight we performed simple experiments to determine the effect of solution concentration (ionic strength) on the dispersion of diamond dust and Cr_3C_2 particles. The effect of wetting agents, one cationic (cetyltrimethylammonium bromide) and the other anionic (sodium dodecylsulfate) was also investigated. The results are tabulated in Table I. As ionic strength increases the coagulation becomes more significant. An anionic wetting agent appeared to obviate the clumping. The data was gathered by visual examination of video tapes recorded with the apparatus of Figure 2B. Different particles, solutions, pH effect and particle shapes (spherical) will be tested in later flights. Knowledge of zeta potentials would be required for a complete study.

40

2. Electrodeposition

A very fast electrodeposition rate at 12 volts (~300 ma/cm^2) at 10^{-2} g from NiBF$_4$ solution gave an x-ray spectrum of only one peak. However, surface enhanced Raman spectroscopy showed it to be an oxide of nickel. All work to date with nickel sulfamate and nickel sulfate solutions with low, moderate and high rates at 10^{-2} g also only shows the cubic face centered pattern of crystalline nickel. However, variations in the peak intensities do not follow a pattern that is explainable. It is possible that our multiple short time (20 seconds) accumulations for 3-5 minutes lead to imprinting of structure and thus do not truly represent what can occur in extended low g. Work with cobalt has shown the tendency for low pH cobalt solutions to give cubic structures and higher pH to give a hexagonal form. Palladium deposited at our highest rate (corresponding to 12V) at 10^{-2} g gave an x-ray pattern consistent with face centered cubic.

References

1. Clyde Riley, H. Dwain Coble, Boon H.Loo, "Surface Coatings and Catalyst Production by Electrodeposition". Annual Report, Consortium for Materials Development in Space, NA6W-812 September 1986.

2. H. S. Carslaw and J. C. Jaeger, Conduction of Heat in Solids, 2nd Ed., p. 75, Oxford Press (1959).

3. R. N. O'Brien and H. Kolny, Canadian J. Chem. 56, 591 (1978).

4. C. Riley, D. Coble and G. Maybee, "Electrodeposition of Metals and Metal/Cermet Composites in Low Gravity", AIAA-87-0510, Reno, Nevada.

5. Ralph N. Adams, Electrochemistry, At Solid Surfaces, Marcel Dekker, Inc. New York, (1969), Chap. 3.

6. N. Guglielmi, J. Electrochem. Soc., 119, 1009 (1972).

7. F. A. Lowenheim, Metal Finishing, 78, No. 1A, 317 (1980).

8. Josef Ehrhardt, a) "Dispersion Electrolysis Under Zero Gravity in the SPACELAB Rocket Program TEXUS IV". Battelle-Institute, BMFT Reference No. 01 QV 219-AK-SN/A-SLN 7910-5, April 1982, b) "TEXUS VII", BMFT Reference No. 01 QV 219-AK-SN/A-SLN 7910-5, November 1983 and c) "TEXUS IX", BMFT Reference No. 01 QV 014-AK/SN, November 1984.

9. Reference 7, page 428.

10. H. Matsueda and B. L. Averbach, Materials Science and Engineering, 23, 1131 (1976).

11. Chwu-Ching Jan and Richard L. McCreery, Anal. Chem., 57, 8, 1763 (1985).

12. C. Riley, H. D. Coble, B. Loo, B. Benson, H. Abi-Akar, and G. Maybee, Polymer Preprints, 28, 2, 470 (1987).

13. K. W. Beach, R. H. Muller and C. W. Tobias, J. Opt. Soc. Am. 63, 559 (1973).

14. F. R. McLarnon, R. H. Muller and C. W. Tobias, J Electrochem. Soc., 59 (1975).

Presentations and Publications

1. G. Maybee, C. Riley and D. Coble, "Microgravity Effects on Electrodeposition of Metals and Metal Cermet Mixtures", GAS Conference, October 1986, Goddard Space Center, Greenbelt MD.

2. C. Riley, D. Coble and G. Maybee, "Electrodeposition of Metals and Metal/Cermet Composites in Low Gravity", AIAA-87-0510, Reno, Nevada

3. B. H. Loo, C. Riley, H. D. Coble and H. Abi-Akar, "Oscillatory Behavior of Electrodeposition of Cobalt", Alabama Academy of Science meeting, Florence, AL, March 1987.

4. C. Riley, H. D. Coble, B. Loo, B. Benson, H. Abi-Akar and G. Maybee, "Electrodeposition and Codeposition Under Low Gravity/Nonconvecting Conditions", _Polymer Preprints_, 2, 470 (1987).

5. C. Riley, H. D. Coble, B. Loo, B. Benson, H. Abi-Akar and G. Maybee, "Electrodeposition and Codeposition Under Low Gravity/Nonconvecting Conditions", (Invited presentation, 194th ACS National Meeting, New Orleans, LA, September 1987.)

Table I

CMDS
UNIVERSITY OF ALABAMA
HUNTSVILLE

MCDONNELL DOUGLAS
ASTRONAUTICS CO.
HUNTSVILLE

KC-135

PARTICLE DISPERSION EXPERIMENTS

IF CLUMPING VISIBLE - YES
IF CLUMPING NOT VISIBLE - NO

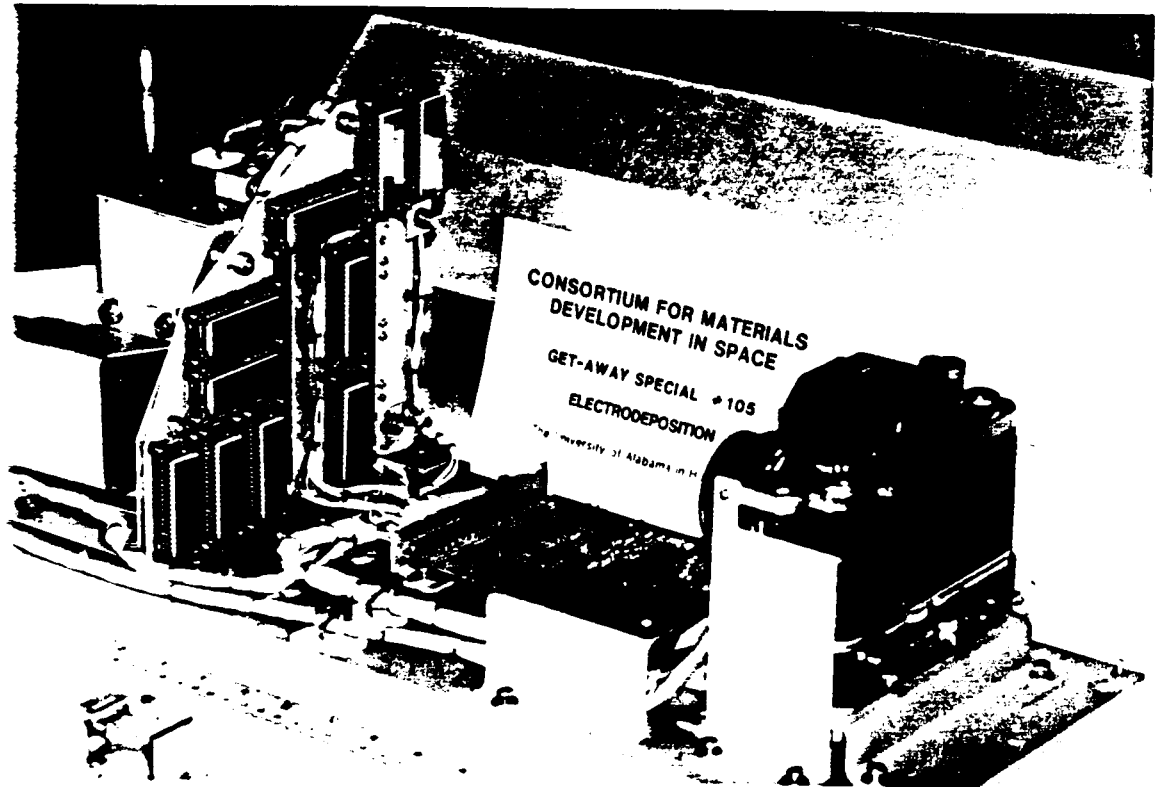| PARTICLE TYPE	$ZnSO_4$ CONCENTRATION	NO WETTING AGENT	(CATIONIC) CTAB	(ANIONIC) SDS
DIAMOND DUST ~ 1μm	.5m	NO	—	—
DIAMOND DUST ~ 1μm	1.0m	YES	—	—
DIAMOND DUST ~ 1μm	1.5m	YES	—	—
Cr_3C_2 ~ 3μm	.5m	NO	—	—
Cr_3C_2 ~ 3μm	1.0m	YES	—	—
Cr_3C_2 ~ 3μm	1.5m	YES	YES	NO

CTAB ≡ CETYLTRIMETHYLAMMONIUM BROMIDE
SDS ≡ SODIUM DODECYLSULFATE

Figure 1.

Low gravity orbitor electrodeposition flight apparatus.

45

Figure 2A.

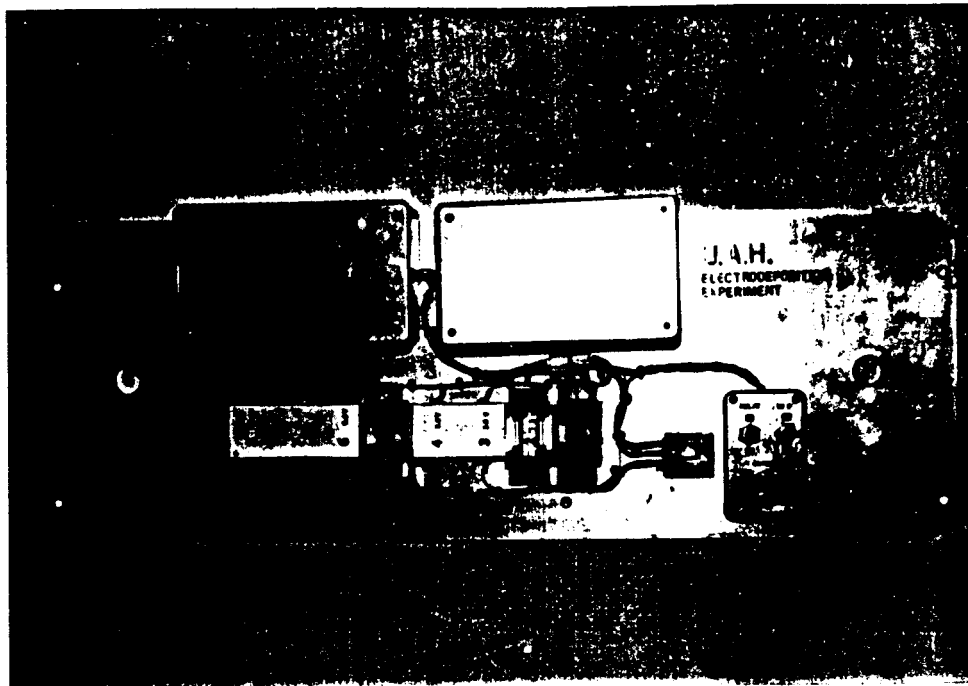KC-135 Electrodeposition apparatus.
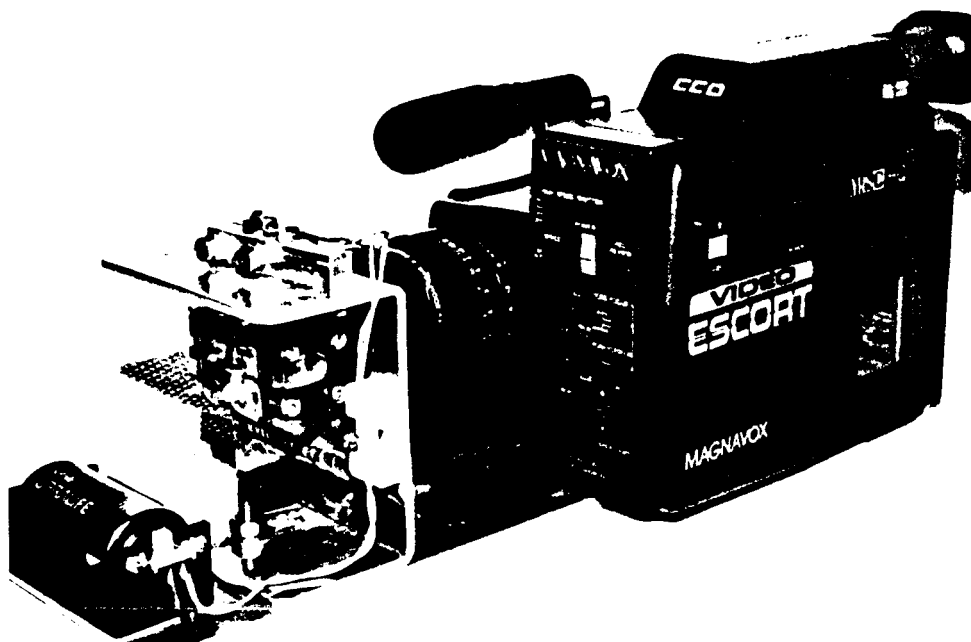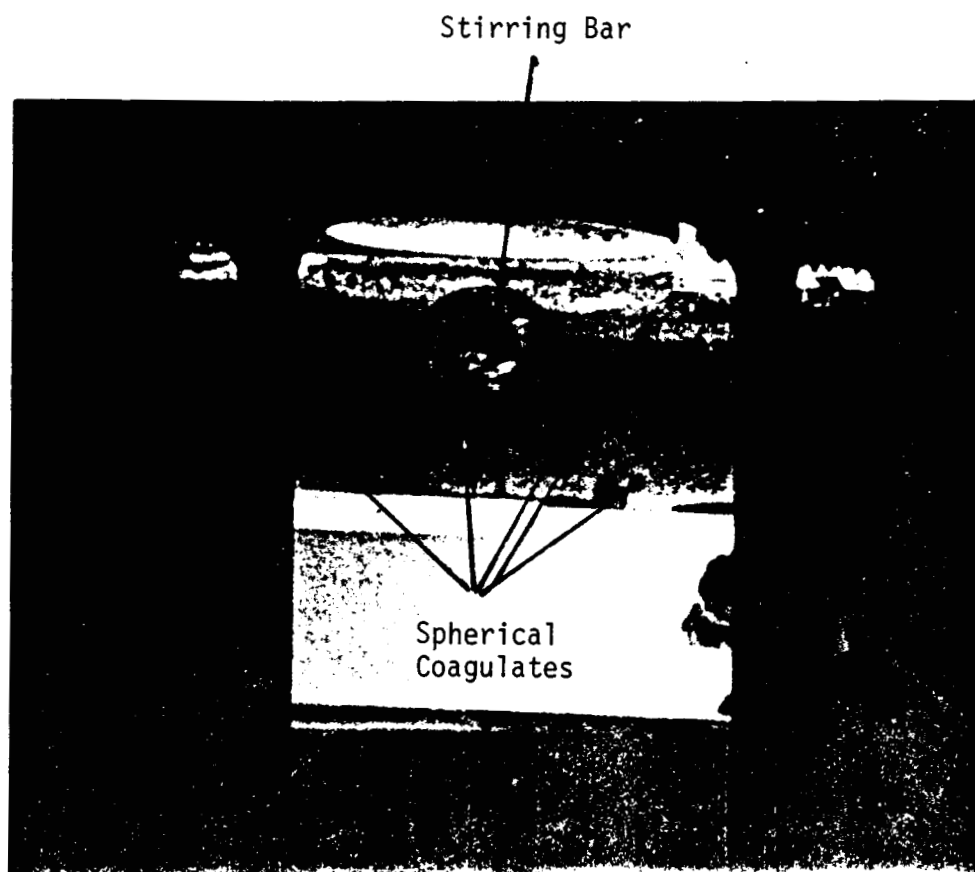
Figure 2B.

KC-135 Particle stirring test apparatus.

Figure 3.

KC-135 Cr_3C_2 stirring experiment at time 20 seconds at 10^{-2} g.

Figure 4. LINEAR SPATIAL ABSORPTION SPECTROPHOTOMETRY FOR CONCENTRATION GRADIENTS
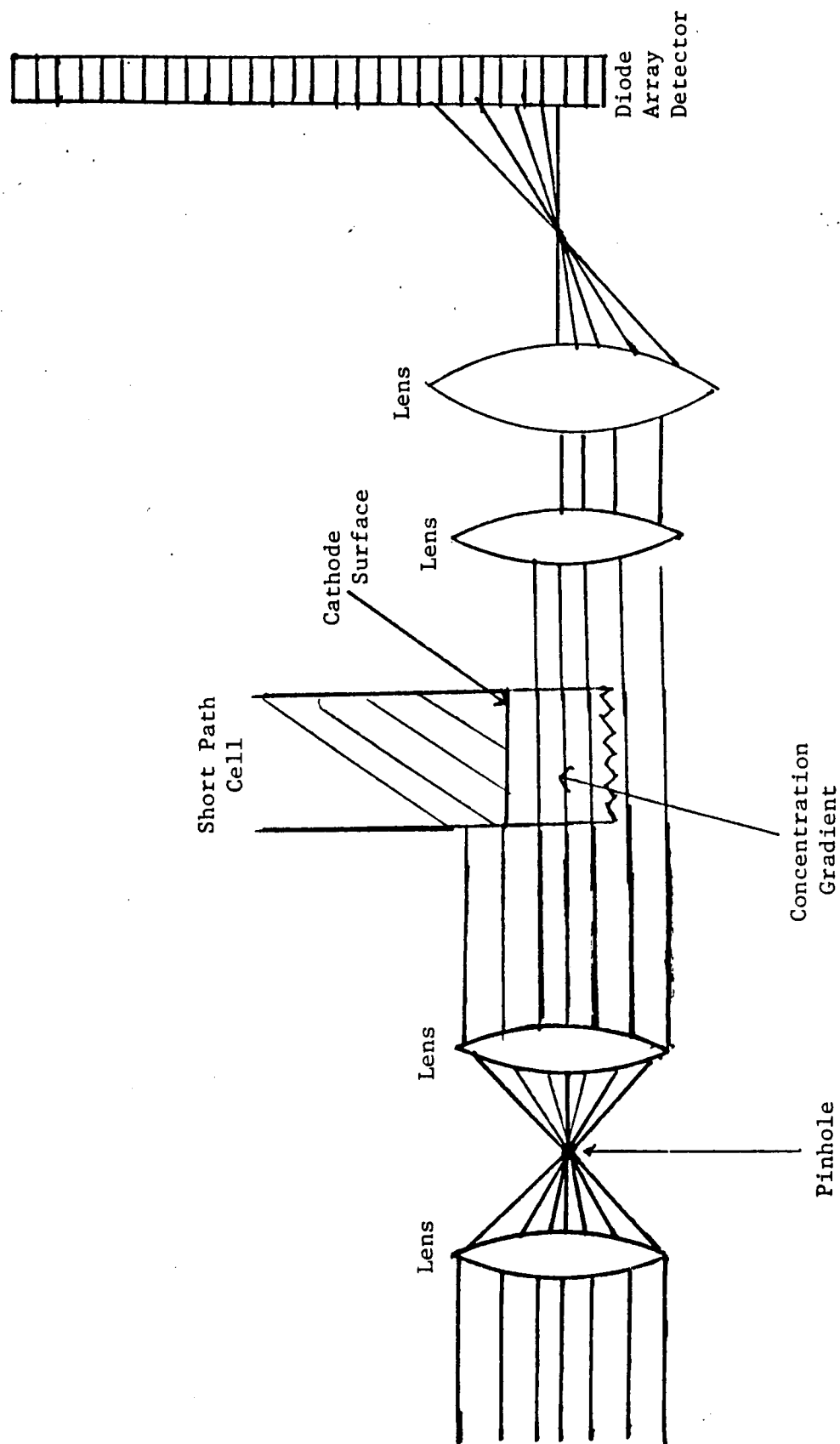
Center: Consortium for Materials Development in Space
         The University of Alabama in Hunstville (UAH)

Project Name: **"Surface Coatings and Catalyst Production by Electrodeposition"**

Subproject Name: **"Mass Transport by Diffusion"**

The University of Alabama in Huntsville
                         James K. Baird

Annual Report: September 15, 1986 to September 14, 1987

* *

Introduction

Mass transport by diffusion is important in electrodeposition and in many other forms of crystal growth occurring in solution.[1] Since the coefficients of diffusion of important species are not always known, especially at temperatures other than 25 C, it is essential to have available apparatus for measuring them.

A convenient device for measuring diffusion coefficients is the diaphragm cell, which has become standard in the field since its introduction in 1929.[2] The heart of any diaphragm cell consists of two well stirred solution compartments on opposite sides of a porous glass frit. When solutions of differing concentration are placed in the compartments, diffusion occurs across the frit. Since the porosity of the frit is not known a priori, the diaphragm cell must be calibrated before it can be used with solutions with unknown diffusion coefficient. In standard practice, the cell is calibrated with an aqueous solution of 0.5 M KCl at 25 C, a system for which the diffusion coefficient has been determined with great accuracy.[3]

For the purpose of determining diffusion coefficients as required for electrodeposition studies and other applications, we have constructed a diaphragm cell and an isothermal water bath. This system is currently being calibrated as described above.

In studying previous work, we found that a rigorous theory for the operation of the diaphragm cell was not available except in the special that case the diffusion coefficient was independent of concentration.[3,4] This situation is usually encountered in practice, however, only in the limit of infinite dilution. At high concentration, most solutions are thermodynamically non-ideal, which causes the diffusion coefficient to be concentration dependent. Since crystals are grown from supersaturated solutions, it is often the high concentration value of the diffusion coefficient which is the most important for interpreting the rate of mass transport observed in the growth process.

In order to extend the applicability of the diaphragm cell to the important high concentration regime, we have developed a rigorous series integration of the equation of motion governing the cell.[5] Let $c_1(t)$ and $c_2(t)$ be the solute concentrations at time t, observed below and above the diaphragm, respectively. If the solution volumes below and above the diaphragm are identical, the mean concentration, $\bar{c} = (1/2)[c_1(t) + c_2(t)]$, is independent of time. Let $D(c)$ be the diffusion coefficient, taken as a function of concentration, and let $\Delta c(t) = c_1(t) - c_2(t)$ represent the concentration difference measured across the diaphragm. We have found that t and Δc are related by the equation,

$$t = A_0 + A_1 \ell n(\Delta c) + A_2 (\Delta c)^2 + A_4 (\Delta c)^2 + \cdots \qquad (1)$$

where the coefficients, A_n, n = 0, 1, 2, $\cdots$, depend upon $D(c)$ and various derivatives of $D(c)$ evaluated at $c = \bar{c}$. The coefficient, A_1, is the most important, since it satisfies the equation,

$$D(\bar{c}) = \frac{1}{\beta A_1} \qquad (2)$$

where β is the cell constant, which is determined by the calibration.

In the high concentration applications, which we envisage, the cell will be started at t = 0 with a certain value of Δc. Subsequently, Δc will be measured as a function of t, and the t $\underline{vs}$ Δc data fitted to Eq.(1) by least squares. The least squares value obtained for A_1 will be used to determine $D(\bar{c})$ at the mean concentration of the cell using Eq. (2). To change the value of $\bar{c}$, the experiment is repeated, starting from a different initial condition. If this procedure is repeated through a sufficient number of cycles, it should serve to map out the entire functional form of $D(c)$.

We note that, when $D(c)$ is independent of c, all coefficients in Eq. (1) except for A_0 and A_1 are identically zero, and our result is the same as that which is well known for this case.[3] As written including the higher order terms, however, Eq. (1) is entirely new and serves to resolve all the ambiguities, which were pointed out more than 30 years ago[4] as being associated with the operation of a diaphragm cell at high concentration. Aside from their intrinsic value in crystal growth, the functional forms of $D(c)$ obtained for various solutes by our method should be useful also in addressing problems in the theory of molecular transport[6] and in the theory of solutions.[7]

Three calibration runs on the diaphragm cell were completed. On the basis of these runs, we may conclude conservatively that the cell constant $\beta = 0.12$ cm^{-2}. Other calibration runs are in progress, which when complete should permit the cell constant to be determined with an accuracy of one percent.

References

1. J. K. Baird, E. J. Meehan, Jr., S. B. Howard, and A. L. Xidis, J. Crystal Growth 76, 694 (1986).

2. J. H. Northrop and M. L. Anson, J. Gen. Physiol. 12, 543 (1929)

3. R. Mills and L. A. Woolf, The Diaphragm Cell, Australian National University Press, Canberra, 1968.

4. R. H. Stokes, J. Am. Chem. Soc. 72, 2243 (1950)

5. J. K. Baird and R. W. Frieden, J. Phys. Chem. (in press)

6. P.O. Lin and A. D. Pelton, Ber. Bunsen-Ges. Phys. Chem. 81, 1243 (1977)

7. J. Leffler and H. T. Cullinan, Jr., Ind. Eng. Chem. Fundam. 9, 84 (1971)

Center: Consortium for Materials Development in Space
          The University of Alabama in Huntsville (UAH)

Project Name: **"Highly Non-Linear Optical Organic Crystals and Films"**

Subproject Name: **"Highly Non-Linear Optical (NLO) Organic Crystals"**

The University of Alabama in Huntsville
                    J. Milton Harris

Annual Report: September 15, 1986 to September 14, 1987

* *

Introduction

This project involves the synthesis and characterization of organic materials having powerful nonlinear optical (NLO) properties and the growth of highly ordered crystals and monomolecular films of these materials. As such we are conducting research in four areas: (1) theoretical design of new materials; (2) characterization of NLO materials; (3) synthesis of new materials and development of coupling procedures for forming layered films; and (4) improvement of the techniques for vapor-phase and solution-phase growth of high-quality organic crystals. This knowledge will form the basis for experiments on growth of these crystals in microgravity.

Recent Activities

Work over the past year has proceeded in all four of the above areas: First, we have continued work with a new apparatus for better defining parameters required to grow crystals of NLO materials by vapor deposition. Second, we have continued development of the chemistry required to prepare new NLO materials and couple them to surfaces. And third, studies into characterizing and

predicting NLO properties have continued. In addition IBM has agreed to cooperate with the Consortium as our partner on this project.

1. Crystal Growth

We have in hand an apparatus for vapor phase crystal growth that will be flown on the Shuttle. This simple apparatus consists of a 4 inch by 0.75 inch glass tube, divided in the middle by an O-ring joint. One half of the tube is the hot end, while the other is the cold end. To provide precise temperature control (+/- 0.05°C), the hot and cold ends have separate wrappings of resistance wire. A stopcock near the center provides access to vacuum. A low energy loss apparatus has been designed by Fran Wessling for incorporation of the tubes into the GAS can. See the appendix for a description of the device.

This apparatus has been used to examine the effects of temperature and pressure on size of crystals from methylnitroaniline (MNA). It has become clear that the best crystals are obtained by slow (2-3 days) crystal growth with small (2-5°C) temperature gaps between hot and cold ends.

We have recently begun collaboration with F. Rosenberger on better defining conditions for crystal growth and on interpreting the results. As a result of this collaboration and our previous experience we have constructed a new apparatus to better control crystal growth. This apparatus has two new features. First, rather than having a cold end, the new device has a cold "sting" made of gold. This permits maintaining the temperature of the entire tube at the "hot" temperature, with the exception of the sting which has its own separate temperature control. With this alteration we should avoid growth of crystals along the walls of the tube. Secondly, the new tube has controlled flow of inert gas down the tube. With this alteration we can control diffusion rates of vapor down the

54

tube. Diffusion rates of the organic material will be measured at various positions in the tube by light scattering.

This apparatus is being used to better define crystal growth conditions for our first shuttle flight with the simple apparatus (described first above). Also, it is our goal to fly a much more sophisticated apparatus such as the Rosenberger device on subsequent Shuttle flights.

As a second part of this work, we have now begun growing crystals of the betaines by solution crystal growth. Preliminary studies appear promising as some crystals have already been prepared. These materials will be used for structure determination by x-ray crystallography and for measurement of the second order nonlinearity (chi-2) by frequency doubling.

2. Synthesis of NLO Materials and Coupling Chemistry

A major interest here is in synthesis and characterization of betaine dyes as NLO materials. The synthetic approaches were described in the previous annual report. We have now shown that these approaches work, and we have prepared four new betaines. The second-order nonlinearity values (beta) for these compounds will be determined by means of the solvatochromic method. All the materials are highly solvatochromatic, and thus from preliminary examination appear to be highly interesting. From this work should come a better understanding of the molecular properties leading to solvatochromism and NLO properties. Additionally, we are in the process of preparing a fifth betaine derivative incorporating an optically active center to ensure crystallization in an enantiomorphous space group.

A second task in this area is to couple betaines to surfaces as monolayers and multilayers. The carboxyl derivative has been synthesized for this purpose

55

and will be used to couple NLO materials to aminated surfaces using techniques we have developed previously.

3.   Theoretical Investigation of NLO Properties and Characterization

Work here continues, in collaboration with J. K. Baird, in two areas. First we are investigating use of the solvatochromic effect for measuring beta values. This theory is now well in hand, and we are using it to characterize betaines and compounds provided by IBM (our new partner). In the second area we are investigating theoretical calculation of beta values by use of additivity principles and quantum mechanical calculations. This work is just beginning and will be described in more detail in the next report.

Center: Consortium for Materials Development in Space
          The University of Alabama in Huntsville (UAH)

Project Name: **"Highly Non-Linear Optical Organic Crystals and Films"**

Subproject Name: **"Electrooptical Organic Materials"**

The University of Alabama in Huntsville
                        Samuel P. McManus
                        Franz Rosenberger
                        John Matthews

Annual Report: September 15, 1986 to September 14, 1987

* *

Introduction

Nonlinear Optics. Devices employing nonlinear optics (NLO) hold great prom-
ise for important applications in integrated optics, optical information proc-
essing and telecommunications. Although inorganics are the standard, the
exceptional merit of organic materials has now been demonstrated. Properly
designed organics possess outstanding optical and electrooptical properties
which will substantially advance many technologies including electrooptical
switching, optical amplification for communications, and parallel processing for
hybrid optical computers.[1] A brief comparison of organic and inorganic materi-
als follows:

Organic (non-resonant)	**Inorganic (resonant)**
Large reactive nonlinearity - - - - - -	Small reactive part
Fast response (< ps) - - - - - - - - - -	Slower response (> 0.5 ns)
Large window (700 - 1600 nm) - - - - -	Narrower window (a few nm)
Poor processing technologies - - - - - -	Good processing technologies
Amenable to molecular engineering - - -	Limited prospects for advances

Polydiacetylenes. Special interest has been recently focused on organic
small molecules[2] and on organic polymers, such as polydiacetylenes.[3] Ease of
design and fabrication is an especially important characteristic with organic
polymers. To date several polydiacetylenes with interesting third-order

57

susceptibilities have been described. Sauteret et. al.[3] found that crystals of the polymeric sulfonate ester called PTS (made from the crystalline diacetylene monomer called TS where R in the structure below is $CH_2OSO_2C_6H_4$-p-CH_3) have third-order susceptibility values comparable to those of inorganic semiconductors or pure germanium.

Generalized Diacetylene and Polydiacetylene Structures

Monomer: R$-$C$\equiv$C$-$C$\equiv$C$-$R

Polymer:
R
 \
  C$-$C$\equiv$C$-$C   etc.
                \
                 R

Wegner[4] is credited with pointing out that polydiacetylenes are members of a novel class of polymers; crystals of the monomer polymerize either with uv or x-ray irradiation or thermally to give highly ordered polymer single crystals. Even though the monomer is sensitive to polymerization, the x-ray single crystal structure of the crystalline PTS monomer has been worked out by Enkelmann[5] and the polymer structure has been determined by Kobelt and Paulus.[6] Crystal structures of diacetylene monomers having substituent groups, R, other than the sulfonate ester group have also been studied. Garito et al[7] have prepared a dinitrophenolate derivative, DNP, [R = $CH_2OC_6H_3$-2,4-$(NO_2)_2$] which thermally polymerizes but does not undergo polymerization under normal x-ray irradiation. Like TS, the crystal structure for the DNP monomer shows that the unsaturated chains of adjacent molecules in the unit cell are positioned so that polymerization requires only slight atomic movement. This is not always the case. It has been demonstrated by several workers that substituent patterns are very important in the molecule's achieving the proper alignment for polymerization.

Knowing that the TS and PTS data require some atomic movement upon polymerization and assuming that the crystal structure probably restricts major atomic reorganization, Baughman[8] suggested that close packing of the monomeric diacetylene residues was essential. A recent report by a group at GTE Laboratories described the properties of thin films prepared by what may be considered a substantially-modified directional solidification device.[9] The description of four-wave mixing experiments, which revealed that indeed these materials have exceptional optical properties[10], is a significant milestone.

Technical Discussion

During this period of performance we have focused our attention on the process of growing crystals of polydiacetylenes as thin films. We have discussed in previous reports the problems with this task. For example, the polydiacetylenes with the best nonlinear optical properties, e.g. the toluenesulfonate polymer, typically crystallize as lozenge-shaped crystals rather than as thin films. Crystals have generally been grown from solution of these materials or, in the case of some urethane monomers, from the melt. We decided to devote some attention to defining diacetylene monomers which are less heat sensitive than the toluenesulfonate and which may be processable by a technique other than solution crystallization. This report will dwell only on the crystal growth studies although some chemical structural studies continue to be performed.

Chemical Structural Studies. We undertook studies to see if modification of the diacetylene's chemical structure is a feasible way to make the materials more processable. Tripathy[11] has reported results of a theoretical study which indicated the types of R groups which would best enhance the optical properties

of the diacetylenes. Therefore we sought to take advantage of his studies by targeting molecules which fit his design criteria while having more acceptable vapor pressures for PVT crystal growth. In this connection we have prepared two new diacetylenes which offer some promise. These materials are made from readily available raw materials and readily undergo polymerization when concentrated or crystallized. The first is a diketone, prepared from the corresponding diol by oxidation:
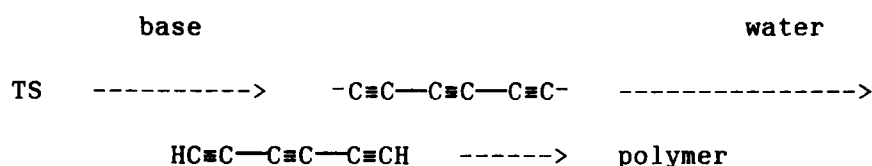
CH3CHOHC≡C—C≡CCHOHCH3   ----> CH3COC≡C—C≡CCOCH3
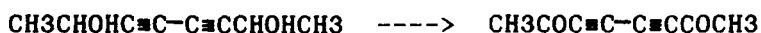
When purified and concentrated, the diacetylenic diketone spontaneously polymerizes to give a dark-colored product.

CH3COC≡C—C≡CCOCH3   -----> conjugated polymer
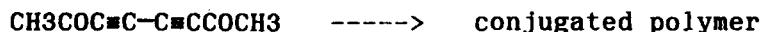
High pressure liquid chromatography showed the material to be a mixture of monomer, oligomers and polymer. No well defined crystalline phase was present yet the conditions of polymerization were far from ideal. A more controlled polymerization may lead to a better quality material. Laser irradiation of the impure form did not substantially change the amount of polymer but seemed to cause some charring. A second new material was inadvertantly prepared in an attempt to replace the tosylate group with other functional groups. Using reaction conditions that we have recently found to be extremely useful for displacement of a sulfonate ester group by good nucleophiles, we attempted to displace a tosylate group with various nucleophiles (e.g. the anions of aromatic amines or alcohols). However, we found that a brownish-black solid was formed which did not incorporate the nucleophile. Thus when we reacted those anionic nucleophiles

60

or simply the dimsyl anion ($CH_3SOCH_2^-$) in dimethylsulfoxide (DMSO) with the monomeric sulfonate ester TS, we apparently obtained the product of elimination rather than the desired substitution. We can account for the results by assuming that a double elimination and deprotonation has occurred, giving the novel triacetylene dianion, as shown below.[12] When the solution of this material is poured into water, polymerization apparently occurs. Since this new material should have a conjugated structure, it may have useful properties yet unknown. Hence further studies of these new materials, and closely related structures, seems warranted.

$$
\begin{array}{ccc}
\text{base} & & \text{water} \\
\text{TS} \quad ---------> \quad {}^-C\equiv C-C\equiv C-C\equiv C^- & ---------------> \\
\end{array}
$$

$$
HC\equiv C-C\equiv C-C\equiv CH \quad ------> \quad \text{polymer}
$$

We also have attempted to make some other diacetylene monomers that suggest that there is a limit to the extent that we can modify the structure. It appears that certain R groups may be so strongly electron-withdrawing that they will separate from the diacetylene framework and give an ionic residue. This has interesting possibilities, but, at the moment, no commercial interest.

Crystal Growth Studies. Crystal growth studies have been carried out with 3,5-octadiyn-1,8-diol, a low melting diacetylene with better thermal stability than the tosylate. With this monomer crystalline thin films have been deposited on glass, polyethylene film, and on copper. The results so far are doubly impressive. Significantly, we are the first to demonstrate that crystalline monomeric films of diacetylenes can be grown using physical vapor transport techniques. The films are colorless and vary in thickness from about 0.005 mm

to 0.1 mm. Not surprisingly, a great deal of difference is found with the various substrates, with each providing some significant data. To date all experiments have been carried out with continuous pumping and with relatively large differences in temperature between the substrate reservoirs and the growth surface. However, much improvement with this system is available. Data reduction from the large number of experiments is continuing. A most important difference sought and observed with the different growth surfaces relates to epitaxial growth potential for this system. The crystalline structure of the diol crystals grown from solution is dominated by hydrogen bonding between hydroxy groups. This prevents the diacetylene units from achieving their maximum interaction and is thought to lead to fragile crystals. We find that a glass surface seems to attract hydrogen bonding to the glass surface and hence the intramolecular hydrogen bonding, at least in the first monolayer, is different. The difference in the growth patterns, which may signal a morhological difference is apparent from observing the initial buildup pattern of the films. With the glass surface the film growth is continuous from the beginning. With the polyethylene surface growth occurs in small crystallites evidence of growth being favored by building on prior nucleation sites. With copper there seems to be a buildup of prior nucleation sites but the growth is not as dramatic as with polyethylene. These studies are continuing with the goal of incorporating our present best film-forming system into a Get Away Special experiment.

Bibliography

1. (a) H. J. Caulfield et. al., eds., Special Issue of <u>Proc. of IEEE</u>, July, 1984; (b) D. Psaltis, ed., Special Issue of <u>Opt. Eng.</u>, Jan, 1984; (c) J. Neff, ed., Special Issue of <u>Opt. Eng.</u>, Jan, 1985; (d) D. J. Williams, ed, "Nonlinear Optical Properties of Organic and Polymeric Materials", Washington: Amer. Chem. Soc. Symposium Series No. 233, 1983.

2. B. F. Levine, C. G. Bethea, C. D. Thurmond, R. T. Lynch, and J. L. Bernstein, <u>J. Appl. Phys.</u>, <u>50</u>, 2523 (1979); G. F. Lipscomb, A. F. Garito, and R. S. Narang, <u>J. Chem. Phys.</u>, <u>75</u>, 1509 (1981).

3. C. Sauteret, J. -P. Hermann, R. Frey, F. Pradere, J. Ducuing, R. H. Baughman, and R. R. Chance, <u>Phys. Rev. Lett.</u>, <u>36</u>, 956 (1976).

4. G. Wegner, <u>Z. Naturforsch.</u>, <u>24B</u>, 824 (1969); <u>Makromol. Chem.</u>, <u>145</u>, 85 (1971); <u>ibid.</u>, <u>154</u>, 35 (1972); for a review, see D. Bloor in "Developments in Crystalline Polymers", D. C. Bassett, Ed., Appl. Science Publ., London and New Jersey, 1982, 151.

5. V. Enkelmann and G. Wegner, <u>Angew. Chem.</u>, <u>89</u>, 432 (1977); unpublished work of V. Enkelmann (1983) cited by M. Schwoerer and H. Niederwald, <u>Makromol. Chem.</u>, <u>Suppl. 12</u>, 61 (1985).

6. D. Kobelt and E. F. Paulus, <u>Acta Cryst.</u>, <u>B30</u>, 232 (1974).

7. A. F. Garita in ref. 1d.

8. R. H. Baughman, <u>J. Polym. Sci., Polym. Phys. Edit.</u>, <u>12</u>, 1511 (1974).

9. M. Thakur and S. Meyler, <u>Macromolecules</u>, <u>18</u>, 2341 (1985).

10. G. M. Carter, M. K. Thakur, Y. J. Chen, and J. V. Hryniewicz, <u>Appl. Phys. Lett.</u>, <u>47</u>, 457 (1985).

11. B. J. Orchard and S. K. Tripathy, <u>Macromolecules</u>, <u>19</u>, 1844 (1986).

12. C. L. Cook, E. R. H. Jones, and M. C. Whiting, <u>J. Chem. Soc.</u>, 2883 (1952).

Center: Consortium for Materials Development in Space
         The University of Alabama in Hunstville (UAH)

Project Name: "Highly Non-Linear Optical Organic Crystals and Films"

Subproject Name: "Theory of Atomic Additivity in Molecular Hyperpolarizabilities"

The University of Alabama in Huntsville
                    James K. Baird

Annual Report: September 15, 1986 to September 14, 1987

* *

Introduction

The non-linear optical properties of molecular crystals depend upon the hyperpolarizabilities of the molecules they contain. Consider an electric field with components E_j, $j = 1,2,3$, measured in a Cartesian system of coordinates. The i-th component, m_i, of the electric dipole induced in this molecule by the field is given by

$$m_i = \alpha_{ij}E_j + \beta_{ijk}E_jE_k + \cdots \qquad (1)$$

where on the right hand side, the double occurrence of a subscript implies a summation over all values (1, 2, and 3) which the index may take on. The second rank tensor coefficient, α_{ij}, is called the ordinary dipole polarizability, while the third rank tensor coefficient, β_{ijk}, is called the first dipole hyper-polarizability.

If the applied electric field oscillates at frequency, ω, the induced dipole moment, m_i, oscillates at frequency ω and also at frequency 2ω. The oscillation at 2ω is the origin of the non-linear optical phenomenon known as frequency doubling. Using the time dependent perturbation theory of quantum mechanics, the part of β_{ijk} associated with frequency doubling is

$$\beta_{ijk}(2\omega) = \frac{2\pi^2}{h^2} \sum_{n,\ell} \left[\mu^i{}_{on}(\mu^j{}_{n\ell}\mu^k{}_{\ell o} + \mu^k{}_{n\ell}\mu^j{}_{\ell o})\frac{\omega_n\omega_\ell + 2\omega^2}{(\omega_n{}^2-4\omega^2)(\omega_\ell{}^2-\omega^2)} + \right.$$

$$\left. \mu^k{}_{on}\mu^i{}_{n\ell}\mu^j{}_{\ell o}\frac{\omega_n\omega_\ell - \omega^2}{(\omega_n{}^2-\omega^2)(\omega_\ell{}^2-\omega^2)} \right] \qquad (2)$$

where the ω_n are resonance frequencies for excitation of the molecule from the ground electronic state to the n-th excited state.[1] The $\mu^\ell{}_{pq}$ are electric dipole transition moments connecting the p-th and q-th electronic states of the molecule and are given by

$$\mu^\ell{}_{pq} = \int \phi_p{}^*(r)\ \mu^\ell \phi_q(r)d^3r \qquad (3)$$

where r represents all of the electronic coordinates, $\phi_p(r)$ is the molecular orbital for the p-th state, and μ^ℓ is the electric dipole moment operator. The subscript, zero, in Eq. (2) refers to the ground state. It is clear from Eq. (3) that, if a molecule is to have a non-zero value for β_{ijk} (2ω), it cannot have a center of symmetry.

In the laboratory, β_{ijk} (2ω) may be determined by laser frequency doubling experiments or indirectly by combining measurements of absorption spectral line strengths with the difference in the absorption frequency and the fluorescence frequency found for the molecule.[2]

This structure contains 3 carbon atoms, 5 hydrogen atoms, one carbonyl oxygen (=O), and one OH. By Landolt's Rule, the molar refraction of propionic acid is given by a linear combination of atoms and bond refractions with coefficients specified by the stoichiometry. Using the table, we write

$$R = 3(2.591) + 5(1.028) + 2.122 + 2.553 = 17.588 \qquad (7)$$

The molecular weight and density of propionic acid are M = 74.08 gm/mole and d = 1.0030 gm/cm^3, respectively. Solving Eq. (5) for n and substituting the molecular weight, density, and the value of R given by Eq. (7), we obtain a predicted value for the refractive index,

$$n = \left[\frac{1 + 2(d/M)R}{1 - (d/M)R}\right]^{\frac{1}{2}} = 1.3877 \tag{8}$$

This is to be compared with the measured value n = 1.3869 reported in the Handbook of Chemistry and Physics.

The Additivity Property for Absorbing Compounds

According to Eq. (2), the hyperpolarizability is a function of frequency. This is called dispersion. Because of the Kramers-Kronig relations, we can expect that a material which is dispersing light is also absorbing it.[7] Where there is dispersion and absorption, the molecular polarizabilities are complex functions of the frequency. This has led us to consider atomic additivity in both the real and imaginary parts of the ordinary and hyperpolarizabilities. This effort is desirable not only from a theoretical point of view, but also because of the existence of a large body of complex refractive index data, which may be used to test additivity principle with the complex valued ordinary dipole polarizability.

To date, we have shown using Maxwell's equations, that if the wavelength of the light is is long compared with the molecular size, the Lorentz-Lorenz equation becomes

$$\frac{\tilde{n}^2 - 1}{\tilde{n}^2 + 2} = \left[\frac{d}{M}\right] \tilde{R} \tag{9}$$

where the complex refractive index, $\tilde{n}$, has real and imaginary parts n and k, respectively, and where the complex valued molar refraction, $\tilde{R}$, has real and imaginary parts, R', and R". Eq. (9) may be used to test the additivity concept on the case of dispersion/absorption.

In the vacuum ultraviolet, both n and k have been measured for a number of compounds,[8] among them being cyclohexane (no carbon-carbon double bonds), cyclohexene (one double bond), and cyclohexadiene (two double bonds).[9] Substituting n and k, molecular weight, and density into Eq. (9), we have solved for $\tilde{R}$ for each compound. Our hypothesis of additivity in the case of these three dispersing/absorbing compounds can be tested in the following way: We let $\tilde{R}_0$, $\tilde{R}_1$, and $\tilde{R}_2$ be the complex valued molar refractions of the compounds with none, one, and two double bonds. Letting $\tilde{H}$, $\tilde{C}_1$, and $\tilde{C}_2$ be the complex valued refractions of the hydrogen atom, the carbon-carbon single bond, and the carbon-carbon double bond, we have assuming the additivity principle,

$$\tilde{R}_0 = 6\tilde{C}_1 + 12\tilde{H} \tag{10}$$

$$\tilde{R}_1 = 5\tilde{C}_1 + 10\tilde{H} + \tilde{C}_2 \tag{11}$$

$$\tilde{R}_2 = 4\tilde{C}_1 + 8\tilde{H} + 2\tilde{C}_2 \tag{12}$$

These three equations are not linearly independent, and we find

$$\tilde{R}_1 = (1/2)(\tilde{R}_0 + \tilde{R}_2) \tag{13}$$

which serves as a check on the additivity principle. We have found Eq. (13) to obeyed within experimental error throughout the entire wavelength region (775 to 1770 Angstroms) where complex refractive index data are available for the cyclic hexanes. This result gives us confidence that the additivity principle extends to dispersive systems in general.

The Quantum Theory of Additivity

A theoretical proof of the additivity idea, nevertheless, would be useful. For non-dispersive wavelengths (e.g., for most organic molecules at the Na D line), the electric field of the light wave may be assumed to be static. Since there are in this case no quantum transitions between states, the variation method of quantum mechanics is applicable and has been used with molecular orbital theory of the dipole moment to demonstrate that the additivity principle applies to the ordinary dipole polarizability in the limit of zero frequency.[10]

We are searching for a similar proof for dispersing systems. Using time dependent perturbation theory, we have found that the real part, $\alpha_{ij}'(\omega)$, and the imaginary part, $\alpha_{ij}'(\omega)$, of the ordinary dipole polarizability satisfy the equations,

$$\alpha_{ij}'(\omega) = \frac{2\pi}{h} \sum_{\ell} \mu^i{}_{0\ell} \mu^j{}_{\ell 0} \left[\frac{(\omega_\ell - \omega)}{(\omega_\ell - \omega)^2 + \frac{1}{4}\gamma_\ell{}^2} + \frac{(\omega_\ell + \omega)}{(\omega_\ell + \omega)^2 + \frac{1}{4}\gamma_\ell{}^2} \right] \tag{14}$$

$$\alpha_{ij}'(\omega) = \frac{2\pi}{h} \sum_{\ell} \mu^i{}_{0\ell} \mu^j{}_{\ell 0} \left[\frac{\frac{1}{2}\gamma_\ell}{(\omega_\ell + \omega)^2 + \frac{1}{4}\gamma_\ell{}^2} - \frac{\frac{1}{2}\gamma_\ell}{(\omega_\ell - \omega)^2 + \frac{1}{4}\gamma_\ell{}^2} \right] \tag{15}$$

The quantity, γ_ℓ, is the rate of decay of the ℓ-th(excited) state of the molecule due to the joint effect of collisions and spontaneous emission. In the

limit $\gamma_\ell \to 0$, $\alpha_{ij}''(\omega)$ becomes the difference of delta functions in accord with Fermi's Golden Rule.[11] We maintain γ_ℓ finite, in both Eq. (14) and (15) to avoid this singularity in the latter.

Eq. (2) is the real part of the first hyperpolarizability and is analogous to Eq. (14) with $\gamma_\ell = 0$. One notes that Eqs. (2), (14), and (15) all contain the same set of transition dipole matrix elements, so that if additivity applies to one, it should apply to all. We propose to demonstrate this by following closely the proof already available in the static case.

Applications

We envisage three important applications of the additivity principle as generalized to dispersing/absorbing systems:

1. We have already mentioned the concept of predicting molecular dipole hyperpolarizabilities from bond and atomic hyperpolarizabilities. Using the concepts demonstrated above for propionic acid and for the cyclic hexanes, we propose to construct a table of bond hyperpolarizability contributions found by solving appropriate linear systems of equations involving measured molecular hyperpolarizabilities. These tables will be used to predict the hyperpolarizabilities of molecules not yet synthesized.

2. The rate of energy loss of a fast charge particle (e.g. proton or alpha) moving through matter is determined by the optical properties of the material.[12] To understand this, one should note that the charge of the particle is the source of an electric field, and because the particle is moving, the field is time varying. However, by Fourier's theorem, a

time varying field may be decomposed into sinusoidal frequency com-
ponents. Individually, these have the same effect on the material as
light. By demonstrating the additivity principle, we shall show that
fast charged particles lose energy in covalently bonded materials by
depositing it in the individual chemical bonds. For a complex material
such as a living cell, there are many types of molecules but a far fewer
number of bond types. By showing that chemical bonds are the fundamen-
tal structure in energy loss, we will greatly simplify the study of the
structure of ionization tracks, which is so important in radiation
biology and chemistry.

3. In a dilute gas, $\alpha''(\omega)$ determines the intensities of spectral lines. In
condensed matter, we have shown that both $\alpha'(\omega)$ and $\alpha''(\omega)$ are involved,
combined in a non-linear way. By demonstrating the additivity prin-
ciple, we shall show that the intensities of spectral lines are deter-
mined by the number and types of bonds in the molecules. This should
permit us to examine regularities in spectra with new insight.

References

1. J. L. Oudar and J. Xyss, Phys. Rev. <u>26</u>, 2016 (1982).

2. N. G. Bakhshiev, M. I. Knyazhanskii, V. I. Minkim, O. A. Osipov, and G. V. Saidov, Russian Chemical Reviews <u>36</u>, 704 (1969).

3. Reference 1, page 2019.

4. A. D. Buckingham and B. J.Orr, Quart. Revs. <u>21</u>, 195 (1967).

5. K. G. Denbigh, Trans. Far. Soc. <u>36</u>, 936 (1940).

6. <u>Handbook of Chemistry and Physics</u>, 59th Edition, 1978/79, page E-356.

7. A. S. Davydov, <u>Quantum Mechanics</u>, Pergamon Press, Oxford, U.K., 1965, page 451.

8. M. W. Williams, D. W. Young, J. C. Ashley, and E. T. Arakawa, J. Appl. Phys. <u>58</u>, 4360 (1985) and references therein.

9. B. ᵀ. Sowers, E. T. Arakawa, and R. D. Birkhoff, J. Chem. Phys. <u>54</u>, 871 (1971).

10. K. J. Miller and J. A. Savchik, J. Am. Chem. Soc. <u>79</u>, 7206 (1979).

11. R. G. Gordon, "Correlation Functions for Molecular Motion" in <u>Advances in Magnetic Resonance</u>, J. S. Waugh, editor, Vol. 3, 1968, page 4.

12. H. Frohlich and R. L. Platzman, Phys. Rev. <u>92</u>, 1152 (1953).

Center: Consortium for Materials Development in Space
        The University of Alabama in Huntsville (UAH)

Project Name: **"Physical Properties of Immiscible Polymers"**

The University of Alabama in Huntsville
                    J. Milton Harris

Annual Report: September 15, 1986 to September 14, 1987

* *

Introduction

This project involves investigation of demixing of immiscible polymers in low-G and applications of this knowledge to: (a) providing a better understanding of the role of phase segregation in determining the properties of polymer blends made from immiscible polymers, and (b) purification of biological materials by partitioning between the two liquid phases formed by solution of the polymers polyethylene glycol (PEG) and dextran in water.

It should be noted that this project has changed directions again in that NASA required Celanese to drop out of the Consortium after they were purchased by a German firm.

Work has proceeded in four areas during the past year:

1. Testing of New Apparatus for Space Flight

2. Extension of Affinity Phase Partitioning

3. Refinement of Polymer Chemistry

4. Demixing of Isopycnic Polymer Phases in One-G

Testing of New Apparatus for Space Flight

F. C. Wessling has worked with us on a redesign of the low-G, phase-demixing apparatus. The new apparatus, which has been constructed, consists of an alumi-

num block containing two rows of six cavities (for a total of twelve chambers).
Each cavity will contain a glass cube (1.6 cm^3) which in turn will contain a
polymer two-phase system and a small stirring bar. Stirring is provided by
small stirring motors with magnets attached to the shafts. Thus there are six
motors along the top of the apparatus and six along the bottom. In our previous
design, stirring was done by passing a shaft and paddle through an O-ring into
the phase system container. By eliminating the O-ring and sealing the container
we should now have a much improved device; leakage and shaft freezing, which
were problems with the old design, are now eliminated. In addition, the new
apparatus has heating wires attached to provide heating (necessary in the GAS
can) and temperature control. We have also purchased a Nikon F3 to be used with
this apparatus.

The apparatus has been flown twice on KC 135 flights, and it performed well.
We are now making slight modifications for automated flight as a GAS experiment.
We are considering modifications to make the apparatus suitable for sounding-
rocket flight.

Extension of Affinity Phase Partitioning

A major interest of ours is in developing the technique of affinity phase
partitioning (with polymer two-phase systems) for eventual use in low-G separa-
tion of cells of commercial importance. Previous work has shown that gravity-
driven demixing of the polymer two-phase systems greatly reduces the efficiency
of phase partitioning on Earth; if this randomizing force were removed from
affinity phase partitioning, a cell separation procedure of perfect selectivity
(no undesired cells would be retained) would be provided. Affinity phase
partitioning, previously developed by us, utilizes an affinity ligand (an

73

antibody) attached to PEG to pull cells into the PEG-rich phase (unwanted cells remain at the interface between the PEG-rich and dextran-rich phases).

Previously, we have applied this technique to purifying red blood cells using antibodies to the cells as affinity ligands. In the present project we have worked on extending this technique by covalently binding protein-A, rather than antibody, to PEG. Protein-A is of interest because it binds antibodies. Thus if protein-A is covalently attached to PEG, exposure to any antibody will provide ready binding, via to the protein-A, of the antibody to PEG. This would greatly simplify the technique since it would remove the necessity of covalently binding every desired antibody to PEG; a single PEG-protein-A preparation could be used for a large number of affinity separations.

We have now covalently coupled PEG to protein-A and have shown that this material will bind to the antibody to human red blood cells and this complex will pull these cells into the top PEG-rich phase. Thus we have greatly simplified the general application of the phase partitioning technique to cell separations.

Work in the past quarter has dealt with application of this technique to purifying megakaryocytes. These are cells which are of interest for future space experiments to test the limits of the technique on large cells for which gravity-driven sedimentation of the cells themselves is a problem. Preliminary results are promising.

Refinement of Polymer Chemistry

For the affinity partitioning procedure it is necessary that we have effective chemistry for coupling PEG to proteins. An additional chemistry requirement is for coupling PEG and dextran to glass to control phase demixing

(discussed below). Thus we have an on-going effort in development of the required polymer chemistry.

1. PEG-Protein Chemistry

We have had a long-term effort in evaluating and developing the chemistry for attaching PEG to proteins. A large segment of this work is now approaching completion. In the last quarter we have completed the bulk of the work necessary to: (a) show the relationship between coupling method and protein activity; (b) understand the effect of organic solvents on protein activity and stability; and (c) show the effect of linking proteins to solid supports (glass). We are now writing up this work.

2. Improvement of Coating Chemistry for Conrol of Wall Wetting

A key part of this research program lies in controlling the demixing rate of immiscible polymers by controlling wall wetting by the immiscible phases. Thus we have been examining the effect of covalently bound dextran on the demixing rate for the immiscible phases formed from solution in water of dextran and PEG. It is obviously critical for this work that the chemistry used to bind dextran to the glass containers be effective. In the past we have evaluated our chemistry by wet chemical methods. A great improvement in this evaluation procedure results from use of X-ray photelectron spectroscopy (XPS or ESCA). With this technique it is possible to directly determine the elemental composition of the surface with great accuracy.

Our method for coupling dextran to surfaces has been to first apply an amine sublayer and then to couple the dextran reducing terminus to this amine group. During the past quarter we have used XPS to greatly improve (factor of three) the thickness of the amine sublayer. Basically this improvement came from leaving the amine reagents on the glass and heating at 120°C. Previously we had been washing the reagents off before heating under the supposition that the reagents were held by hydrogen bonding (as published in the literature).

In the next quarter we will apply the XPS technique to evaluate coupling of dextran to the amine sublayer.

Demixing of Isopycnic Polymer Phases in One-G

We have been making a major effort to better understand the gravitational inputs to phase demixing. The question here is: what are the forces which lead to separation or demixing of two stirred but immiscible liquids in the absence of gravity-driven sedimentation? To advance work in this area we will quantify the phase demixing of isopycnic phase systems. The apparatus for studying this process has been assembled (consisting of a Nikon F3 with motor drive and data back, and a 2 in. by 2 in. thermostatted cell to contain cuvettes holding two-phase systems). We have obtained quality photographs of the phase demixing process as a function of time. Now we are working on automation of the characterization process (i.e., determination of the growth rate of droplets or domains) by use of an Omnicon Scanner. In addition we are examining the effect of polymeric wall coatings (dextran in particular) on the rate of demixing; the goal is to control the rate and to control which phase (dextran-rich or PEG-rich) goes to the center of the cuvette. Coating effects are observed, but it would be premature at this point to attempt quantitative description of these effects.

Contact-angle measurements are also being done, as part of another project, to aid in understanding the coating effects. These studies indicate that a dextran wall coating will lead to the dextran-rich phase against the wall of the cuvette.

Center: Consortium for Materials Development in Space
          The University of Alabama in Hunstville (UAH)

Project Name: "High Temperature Superconductors"

The University of Alabama in Huntsville
              Maw-Kuen Wu

Annual Report: September 15, 1986 to September 14, 1987

* *

Introduction

Our laboratory was the first in the world to develop a material with a tran-
sition temperature to superconductivity (Tc) above the temperature of liquid
nitrogen. See Appendix I for a copy of the original paper describing the work.
Despite efforts by other well-known laboratories around the world there still
have been no other major breakthroughs eclipsing our work. This puts us in a
good position to continue our leading role in this area.

The two principal objectives of our present work are to develop materials
that superconduct at higher temperatures and to better understand the mechanisms
behind high temperature superconductivity. To achieve these goals we are carry-
ing out detailed experiments on the thermal reaction, structure, and physical
properties of materials that exhibit superconductivity at high temperatures.

If the results of our studies lend credence to some theories now under
consideration, we may wish to combine immiscible alloys with proper normal state
properties, such as resistivity, crystal structure, and presence of appropriate
excitation. If this is the case we will develop a plan to produce
superconducting materials in the freefall environment of space.

Areas of Study

1. Development of high-Tc superconductors.

Our breakthrough work evolved from the knowledge that pressure has an effect on the transition temperature of the La-Ba-Cu-O compound. We decided to simulate a high pressure environment by replacing the Ba and La with other differently-sized atoms, thereby changing the interatomic distances. After several configurations we estimated an optimal chemical composition of $Y(1.2)Ba(0.8)CuO(4)$. On January 29, 1987, using this formula, we created the first superconductor in a liquid nitrogen environment, approximately 95 K. Subsequent work has raised the Tc to 98 K.

Recent work has demonstrated that Yttrium can be replaced with a wide variety of rare earth elements and the Tc will still remain around 90 K. Others the field claim to have achieved a Tc as high as 240 K, although these results are unstable, inconsistent, and not reproducible.

2. Understanding the mechanisms behind superconductivity.

The complexity of the compounds involved makes understanding the mechanism of superconductivity difficult, but it is this understanding that will be required to make stable superconductors at high Tc ranges. It has been determined that the traditional theories of superconductivity, primarily the theory of electron-phonon interaction, are insufficient to explain the processes we are observing, but we are finding some tendencies that appear to be related to the superconductivity effect.

Our research indicates that the appearance of superconductivity depends on the heat treatment process, the size of the divalent (Ba) and trivalent (Y) atoms, and the crystal structure, which may be related to the size of the ions.

The following research is being initiated to study these and other aspects of the superconductivity mechanism:

   a) Investigation of the thermal processes by simultaneously monitoring the weight loss, the thermal reaction, and the chemical species involved in sample preparation.

   b) Investigation of the Ionic Size Effects through further substitutions and partial substitutions of the divalent and trivalent constituents of the compounds.

   c) Study of possible infrared electronic excitation at room temperature and at low temperatures.

The CMDS project in superconductivity for FY 1988 will have three parts. First, Dr. M. K. Wu and his associates will continue to investigate basic material questions and the particular properties of these materials. Such investigations are of course fundamental to all future applications. This will be a laboratory effort. Second, a team of other CMDS investigators will follow the development of superconductivity applications and devices. They will also study and summarize the potential use of such devices in commercial space systems. This study will include an examination of the lowest temperatures attainable on spacecraft by passive cooling techniques. This examination will involve another material question, namely what surface treatments on radiation surfaces produce the lowest temperatures. Thermoelectric systems may also be investigated for their possible use on spacecraft to cool superconducting devices.

Third, appropriate industrial contacts and interfaces will be established. This will have the objective of arranging industry participation in this project

by FY 1989. Although UAH has already had many discussions with industries, a project agreement is premature under the very fluid circumstances that currently exist.

Papers Published

1. M. K. Wu, J. R. Ashburn, C. J. Torng, P. H. Hor, R. L. Meng, L. Gao, Z. J. Huang, Y. Q. Wang, and C. W. Chu, "Superconductivity at 93K in a New Mixed-Phase Y-Ba-Cu-O Compound System at Ambient Pressure," Phys. Rev. Lett., March 2, 1987.

2. P. H. Hor, L. Gao, R. L. Meng, Z. J. Huang, Y. Q. Wang, K. Forster, J. Vassilious, C. W. Chu, M. K. Wu, J. R. Ashburn, and C. J. Torng, "High-Pressure study of the New Y-Ba-Cu-O Superconducting Compound System," Phys. Rev. Lett., March 2, 1987.

3. C. W. Chu, P. H. Hor, R. L. Meng, L. Gao, Z. J. Huang, Y. Q. Wang, J. Bechtold, D. Campbell, M. K. Wu, J. Ashburn, and C. Y. Huang, "Superconductivity at 98K in the Y-Ba-Cu-O Compound System at Ambient Pressure," to appear in Phys. Rev. B 1987.

4. P. H. Hor, R. L. Meng, C. W. Chu, M. K. Wu, E. Zirngiebl, J. D. Thompson, and C. Y. Huang, "Switching Phenomena in a New 90-K Superconductor," Nature, May 1987.

5. E. Zirngiebl, J. D. Thompson, C. Y. Huang, P. H. Hor, R. L. Meng, C. W. Chu, and M. K. Wu, "Magnetic Studies of High Tc Superconducting $(La(0.9)Sr(0.1))(2)CuO(4-y)$," Appl. Phys. Comm., 7 (1&2), 1-8 (1987).

6. M. K. Wu, J. R. Ashburn, C. J. Torn, G. L. E. Peng, F. R. Szofran, P. H. Hor, and C. W. Chu, "Study of High Tc 76 $Ba(2-x)$ $Sr(x)$ $Cu(3)$ $O(y)$ Compound System," MRS Symposium on High Temperature Superconductivity, ed. by D. B. Gubser & M. Schluter (North Holland 1987), P. 69.

7. C. W. Chu, P. H. Hor, L. Gao, Z. J. Huang, J. Bechtold, M. K. Wu, and C. Y. Huang, "Superconductivity Above 90K in the New $ABa(2)Cu(3)O(6+x)$ System," MRS Symposium on High Temperature Superconductivity, ed. by D. B. Gubser & M. Schluter (North Holland 1987), P. 15.

III. TASKS

Center: Consortium for Materials Development in Space
          The University of Alabama in Hunstville (UAH)

Task Name: **"Powdered Metal Sintering and Infiltration"**

Industrial Participant: Teledyne Brown Engineering
                           300 Sparkman Drive
                           Huntsville, AL
                           Tripty Mookherji

The University of Alabama in Huntsville
                           James E. Smith, Jr.

Annual Report: September 15, 1986 to September 14, 1987

* *

Center: Consortium for Materials Development in Space
          The University of Alabama in Hunstville (UAH)   **N88-11870**

Task Name: **"Cast Iron Freezing Mechanisms"**

Industrial Participant: Deere and Company
                           Technology Center
                           3300 River Dr.
                           Moline, IL   61265
                           N. P. Lillybeck

The University of Alabama in Huntsville
                           James E. Smith, Jr.

Annual Report: September 15, 1986 to September 14, 1987

* *

Introduction

These two tasks are being worked by the same investigator in his metals lab-
oratory using essentially the same equipment. Consequently, they are being doc-
umented in one report rather than in separate reports.

This task has focused on liquid phase sintering and infiltration studies of
refrac ory metals and metal composites. Particular emphasis is being placed on
those powdered metal compacts which produce liquid alloys on sintering. For
this class of materials, heating to a two phase region causes the constituent

C · 2

83

components to react, forming an alloy liquid which must wet the solid phase. Densification is initially driven by the free energy effects which cause rapid rearrangement. Further densification occurs by evaporation and condensation, surface diffusion, bulk flow, and volume diffusion.

In unit gravity, sedimentation causes stratification within the sample that results in a non-uniform coarsening of microstructure. Sintering, in a reduced gravity environment, should produce a smaller grain size, a more uniform microstructure possibly with less voids or defects, and improved mechanical properties.

Many of the most interesting liquid phase sintered materials generally include a refractory metal or ceramic which is sintered or infiltrated at temperatures in the range of 1000 - 1800°C. this requires a furnace capable of melting such materials while maintaining an inert or slightly reducing atmosphere during the sintering or infiltration operation.

Potential uses for liquid phase sintered products include bearings, magnetic materials, electrical brushes and contact points, cutting tools, irregular shaped mechanical parts for high stress environments, and possibly new and improved catalysts for chemical production. Space processing in the areas of uniform cutting tools, magnetic materials, and supported inter-metallic alloy catalysts offer the greatest research and development potential.

Furnace Completion

The construction and retrofit of a TEM-PRES corporation high temperature electric furnace has been completed. Only minor technical problems, as will be described below, remain unresolved. This furnace along with numerical modeling

of both isothermal and directional solidification modes, has increased the over-all understanding of furnace design, application, control, and integration for space processing systems.

Updated Furnace Control Program

An updated control program was developed for the high temperature sintering furnace. This program was developed to provide complete interactive or auto-matic control of the furnace as needed. Since this furnace works at the upper margin of electrical furnace performance, an adaptive computer control scheme was required for rapid heating during initial stages, with more critical control as the furnace achieves its final operating temperature. The program writes a complete experimental history of the furnace operating parameters and processing temperatures to computer disk.

Initial Furnace Performance Testing

The furnace o-ring seals, failure of which was discussed in a previous report, were replaced and tested, achieving the desired performance. The fur-nace was heated to 250°C to test the control program and power systems. To date, we have limited the testing to operating temperatures below 300°C. To operate the furnace at temperatures above 300°C, a hydrogen reducing environment must be used or the molybdenum heating coils will oxidize, becoming unusable. For safe operation approximately 50 cc/min of 5% H_2-95% N_2 or 5% H_2-95% He gas mixture must flow over the coils. Attempts were made to find rotameters with small capacity to mix pure $H2$ and inert carrier gases. The only commercially available flowmeters found capable of providing the hydrogen rates were mass flowmeters. Due to the high cost of these flowmeters, a decision was made to

use premixed gases. This required a slight modification of the gas regulation system to permit the use of premixed gases. With this modification now complete, tests will be conducted near the furnace limits.

Several hardware and software modifications were accomplished to improve both furnace temperature control and positioning. A linear bearing guide was designed, constructed, and installed to improve crucible alignment within the furnace, increase the maximum furnace translation rate, and eliminate potential damage to the crucible during furnace translation. Several moderate temperature experiments were conducted at temperatures less than 800°C to test the validity of the temperature control routines. One sintering experiment was attempted on a precompacted Aℓ sample. It was determined after this experiment that additional data will be required on both positioning and temperature profiles. To expand the number of temperature measurements, preliminary testing of an additional data acquisition board and signal conditioner was performed. The data acquisition board was tested at a communication distance of 26' which is 16' beyond the communication distance recommended by the manufacturer. The test was successful and will permit the installation of up to 16 additional thermocouplers. The temperature measurement, furnace control, and positioning programs are being combined into a system program.

Development of a New Die and Pre-Sintering Environmental Chamber

A pre-sintering environmental chamber was designed and built to permit powdered metal compact preparations under vacuum or a reducing atmosphere at temperatures higher than the commercially available system. The white iron powder studies to be conducted for John Deere, Inc., along with several other materials currently being considered, require either vacuum or a reducing environment to

86

reduce oxidation during preparation. The pre-sintering environmental chamber, shown in Figure 1, encloses the test cylinder in a controlled environment. A high temperature resistance heater, capable of temperatures to approximately 1000°C, surrounds the test cylinder body. To reduce the heat loss in the axial directions, cartridge heaters were installed in both the base of the chamber and plunger extension as shown in Figure 1. The upper operating temperature of this prototype configuration will be limited to approximately 600°C since the chamber base was constructed from aluminum. To extended the upper temperature range, a base made of stainless steel may be needed. Temperature measurement and control techniques along with operating procedures are currently being developed for this unit.

A new test cylinder, with a 0.25 inch diameter bore, was constructed to provide samples for testing in the Rapid Melt/Quench Furnace, currently under development, aboard the KC-135. An initial plunger made of 316 stainless steel was tested. This plunger would not tolerate the stress created at 5000 lbs applied pressure. A modified plunger made of case-hardened steel corrected the problem. With the development of the Rapid Melt/Quench Furnace, the test cylinder, and pre-sintering chamber, we now have the necessary elements to pre-screen samples in a low gravity environment.

The 0.25 inch bore test cylinder along with the 2 cm bore and 1.25 inch bore test cylinders permits the preparation of 0.25 inch, 2 cm, and 1.25 inch diameter samples up to 7 cm long. These test cylinders can be used in the environmental chamber to prepare powder metal samples at sintering pressures exceeding 25 tons, temperatures up to 600°C, and vacuum or reducing atmospheres, for use in the high temperature furnace.

Further, during the next reporting period, we hope to complete the sample pre-sintering experimental apparatus, making refactory sintering experiments possible.

Pre-Sintered Sample Preparation

Powder metal sample preparation procedures have been developed to insure sample uniformity. The powder metal is first sieved to separate a specific particle size range. The test cylinder body, plunger, and base are then cleaned using a caustic solution and rinsed with distilled water. The parts are then hot coated with a sodium sterate and water solution to help prevent galling during the pressing operation. The sterate solution was prepared by mixing 18 gm of sodium sterate with 500 ml water while heating to 85°C to dissolve the sterate. The press parts are immersed in the solution and cured in air prior to use. When cured, the pressing parts have a thin film of sodium sterate which melts at high temperatures to lubricate the die.

For each material studied the pre-sintering temperature, applied pressure, and pressing time must be determined experimentally. The low gravity reactive sintering studies will a require porous refractory metal skeleton of tungsten or tungsten-carbide, which will be coated with and in-situ formed intermetallic alloy. The uniformity of the pre-sintered skeletal material is determined by measuring the material's void fraction as a function of position. To determine the void fraction distribution of the pre-sintered compact a Reichert metallurgical microscope has been integrated with New Brunswick Scientific Co., Inc. Biotran III imaging system, as shown in the photograph in Figure 2.

The Biotran III is a precision instrument designed to automate particle counting and area measurements in an image plane. A high resolution vidicon TV

camera system is coupled to a 4-digit numerical display to count particles or
any distinct separately bounded group of positive or negative image areas in a
field of view. The Biotran III then calculates the ·rcentage ratio of either
positive to negative or negative to positive areas in the field of view. To
fully utilize the Biotran III to experimentally measure the void fractional area
of a powder metal compact, the contrast between the voids and polished metal
surface must be enhanced. This is accomplished by blacking the voids to enhance
contrast.

To test the integrated imaging system, several 2 cm diameter aluminum com-
pacts were pre-sintered using the environmental chamber at room temperature.
Three 16 gm Al samples were pre-sintered at 10,000 lbs applied pressure for 30
minutes, 1 hour, and 2 hours, respectively. The 30 minute and 1 hour cylindri-
cal samples were cut in half lengthwise using a metallurgical saw. The samples
were polished using standard metallurgical techniques, coated with a fine parti-
cle black paint, and repolished to retain the paint within the pores. The
Reichert metallurgical microscope and Biotran III imaging system was then used
to determine the porosity of the sample as a function of position. A photograph
of the aluminum sample as imaged by the above system is shown in Figure 3.
Darken areas, outlined in white by the image processor are voids. The Biotran
III ratios the two image fields as discussed above. This ratio was then used to
determine the void fraction. A representative plot of porosity as a function of
position for the 30 minute pre-sintered aluminum sample is shown in Figure 4.
Samples were found to be more compact near the plunger end of the sample with
this difference diminishing as the sintering time was increased. A study to
determine optimal pre-sintering conditions is currently underway.

Future Plans

With furnace design, interfacing, and operational verification virtually completed, initial testing on lower melting sintered materials such as Al-Fe and Cu-Si will continue. Once the controls and measurement systems on the environmental chamber are completed, the John Deere materials along with the reactive sintering of Fe-Ti in a refractory matrix of tungsten and tungsten-carbide will be studied.

In coming months, an axial and radial profile of the furnace will be obtained at several operating temperatures. These profiles will be measured in all three zones, namely the isothermal zone and the cold over hot and hot over cold gradient zones. Once mapped, a better understanding of the sample operating conditions, gradients, etc. will permit more rapid sample analysis. We will continue our test on AL until we can confirm these operating conditions.
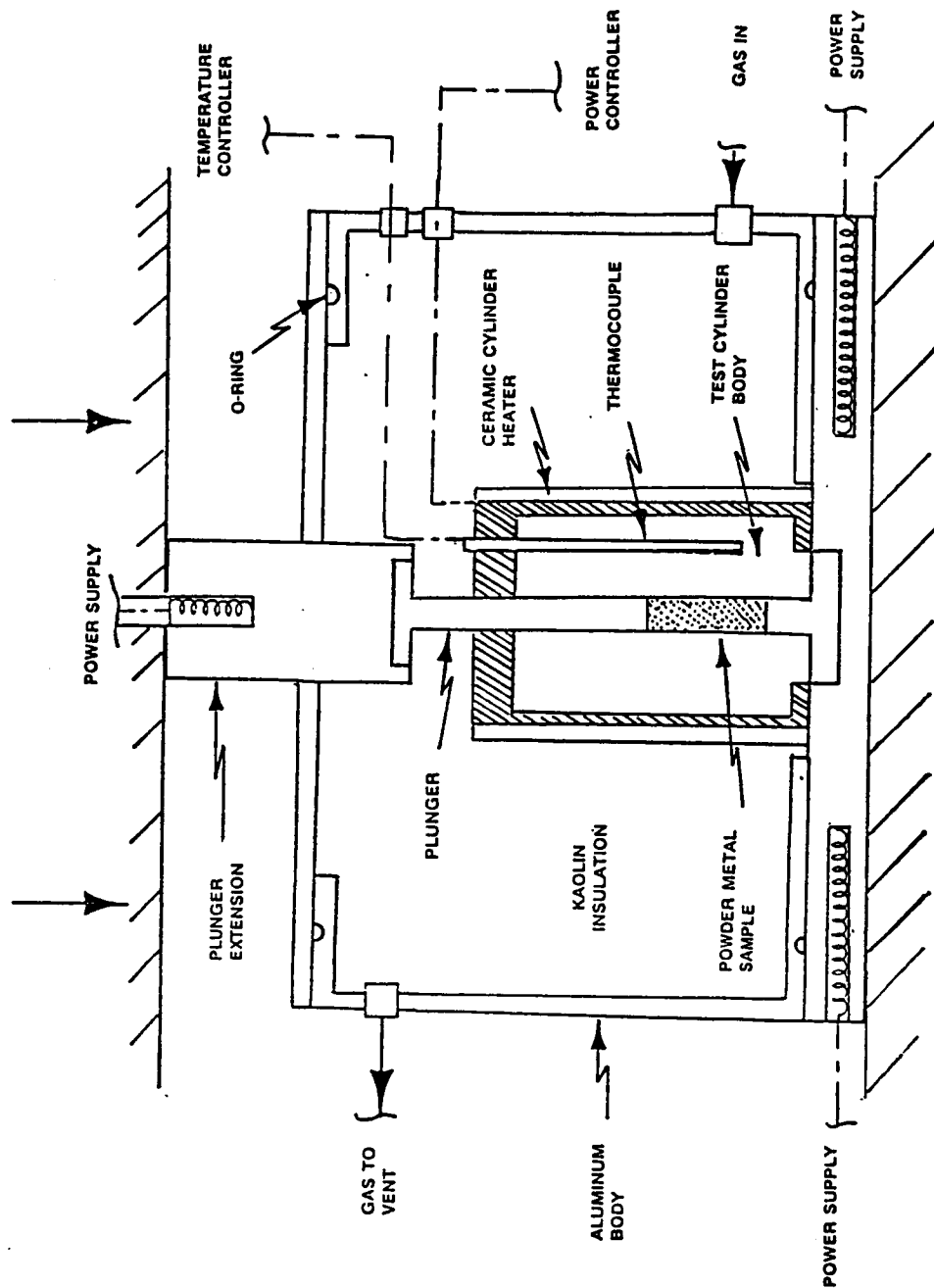
Figure 1. Detailed Drawing Showing the Various Components of the Pre-
Sintering Environmental Chamber Currently Under Development.

91

Figure 2. Photograph of the Reichert Metallurgical Microscope Integrated with the Biotran III Imaging System.
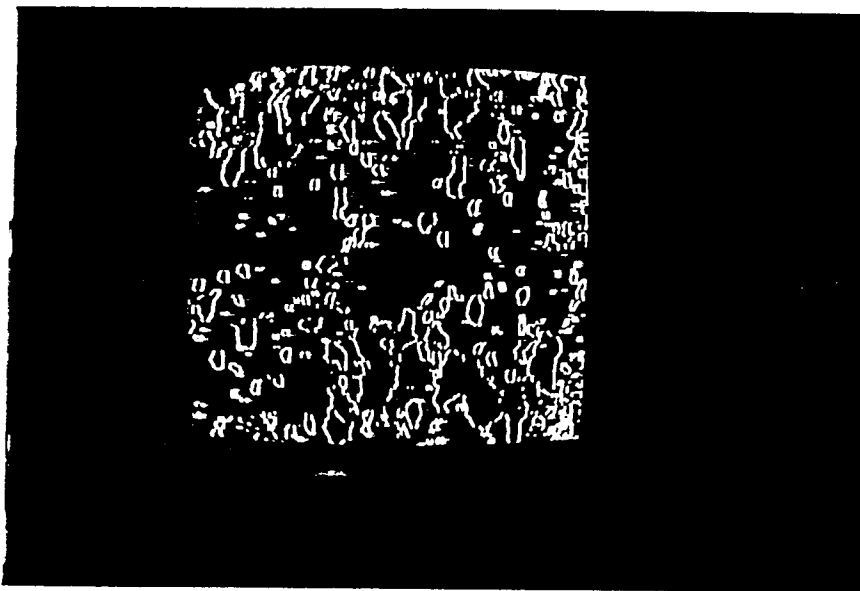
Figure 3   Photograph of the Biotran III Image of a Pre-Sintered Aluminum Sam le.
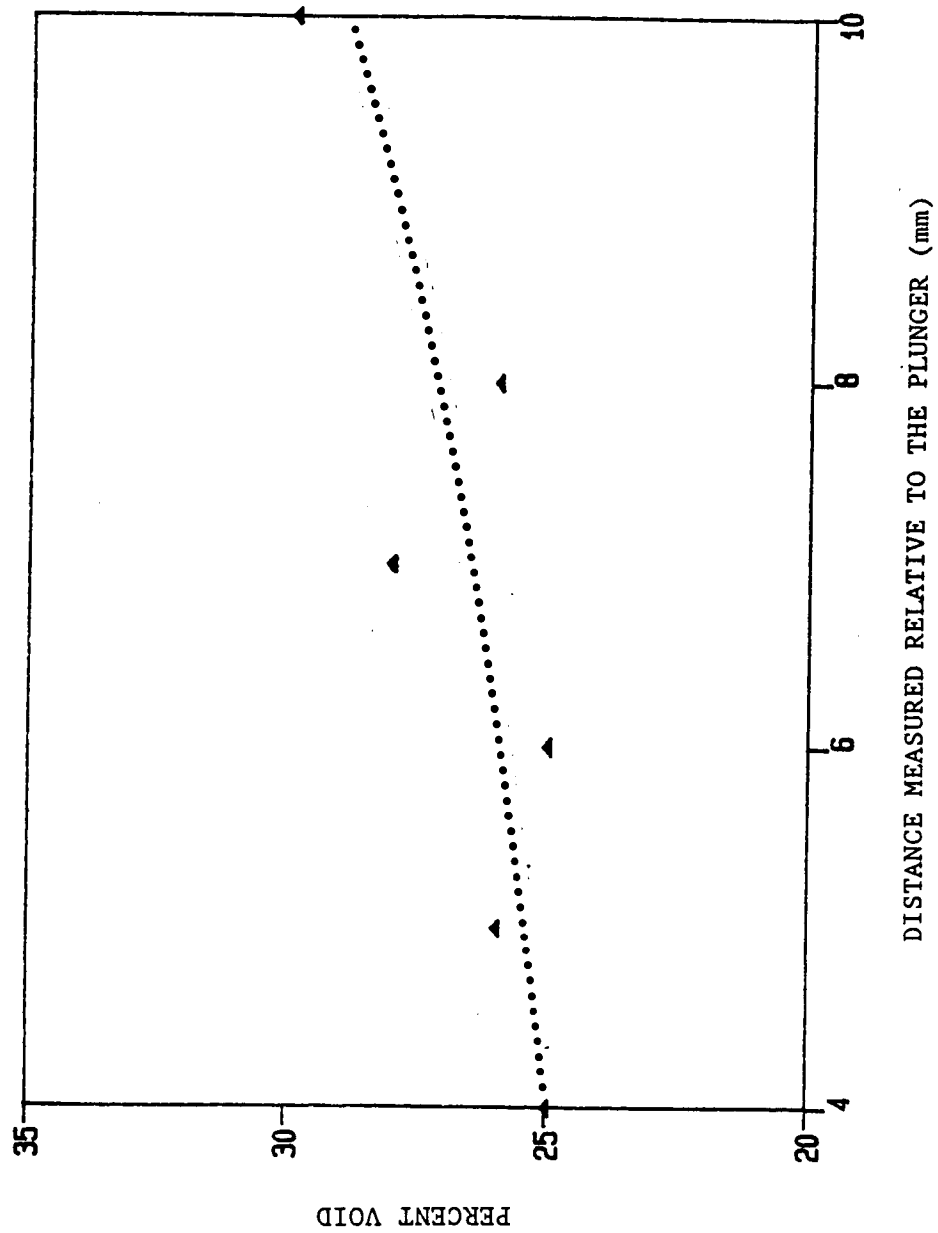
Figure 4. Void Fraction Distribution of a Pre-sintered Aluminum Sample.

93

Center: Consortium for Materials Development in Space
        The University of Alabama in Hunstville (UAH)

Task Name: **"Wake Shield"**

Industrial Participant: Wyle Laboratories
                            P.O. Box 1008
                            Huntsville, AL   35807-5101
                            Tommy Bannister

The University of Alabama in Huntsville
                            Gerald R. Karr

Annual Report: September 15, 1986 to September 14, 1987

* *

Introduction

Progress has been made on the modeling of the flow field around a wake shield using a recently obtained code based on the Mote Carlo method. The code is the original work of Dr. Bird of The Department of Aeronautical Engineering, University of Sydney, New South Wales, Australia. Dr. Karr has been in close communication with Dr. Bird and advice on needed changes has been obtained. The following discusses the code, the modifications needed, and the plans for making the changes.

The direct simulation Monte Carlo method is a method for solving the Boltzman Equation using an approximation to the collision integral term. The collision integrand is evaluated for randomly selected values of its arguments and the summation will approach the integral for large enough samples. The collision effects may be modeled for either hard sphere or various power law potentials. The convective side of the Boltzman equation is approximated over a time step using a simple trajectory calculation of molecules as they travel through the domain of interest. The Bird code is widely use in rarefied gas

94

flow calculations and should be useful in the simulation of the wake shield flow problem. The boundary conditions for the code are the changes required for our application.

The domain boundary conditions are of importance in the application of the Bird code in order to properly represent the effect of the gas-surface effects on the shield. The results we have obtained to present show a region of enhanced density in front of the shield due to the thermalization of ambient molecules that hit the shield. After hitting the shield the velocity is likely reduced to a much smaller value than the 8-km/s incident value. This reduction in velocity coupled with possible directional effects of the surface interaction makes the shield boundary an important surface in the calculation. Presently we use a very simple model of the gas-surface interaction and see a considerable build-up of molecules in front of the shield. This region of enhanced density interacts with the incident flow to cause scattering into the high vacuum region behind the shield. Since this effect could be a limiting factor on the vacuum that can be obtained, we have begun to modify the Bird program to take into account more realistic gas-surface interaction results that have been described in previous reports.

Our plans for modifying the Bird code will require that the method used in the calculation of the effect of collision with the solid boundaries be changed. We are presently working with Dr. Bird to best handle these changes. The work will require that the experimentally determined interaction be modeled in a parameter form that can be randomly sampled. Work has begun on this effort and results should be available during the next reporting period.

Another change in the Bird program that is being addressed is the need to give results in the form of directorial flux rather than number density. The use of directional flux is of more importance to the region behind the shield so that the orientation of experiments can be studied. We have discussed this modification with Dr. Bird and expect to have results available by the next reporting period.

APPENDIX I

SUPERCONDUCTIVITY PAPER

Superconductivity at 93 K in a New Mixed-Phase Y-Ba-Cu-O Compound System at Ambient Pressure

M. K. Wu, J. R. Ashburn, and C. J. Torng

Department of Physics, University of Alabama, Huntsville, Alabama 35899

and

P. H. Hor, R. L. Meng, L. Gao, Z. J. Huang, Y. Q. Wang, and C. W. Chu[a]

Department of Physics and Space Vacuum Epitaxy Center, University of Houston, Houston, Texas 77004

A stable and reproducible superconductivity transition between 80 and 93 K has been unambiguously observed both resistively and magnetically in a new Y-Ba-Cu-O compound system at ambient pressure. An estimated upper critical field $H_{c2}(0)$ between 80 and 180 T was obtained.

The search for high-temperature superconductivity and novel superconducting mechanisms is one of the most challenging tasks of condensed-matter physicists and material scientists. To obtain a superconducting state reaching beyond the technological and psychological temperature barrier of 77 K, the liquid-nitrogen boiling point, will be one of the greatest triumphs of scientific endeavor of this kind. According to our studies,[1] we would like to point out the possible attainment of a superconducting state with an onset temperature higher than 100 K, at ambient pressure, in compound systems generically represented by $(L_{1-x}M_x)_aA_bD_y$. In this Letter, detailed results are presented on a specific new chemical compound system with $L=Y$, $M=Ba$, $A=Cu$, $D=O$, $x=0.4$, $a=2$, $b=1$, and $y \leq 4$ with a stable superconducting transition between 80 and 93 K. For the first time, a "zero-resistance" state ($\rho < 3 \times 10^{-8}$ Ω-cm, an upper limit only determined by the sensitivity of the apparatus) is achieved and maintained at ambient pressure in a simple liquid-nitrogen Dewar.

In spite of the great efforts of the past 75 years since the discovery of superconductivity, the superconducting transition temperature T_c has remained until 1986 below 23.2 K, the T_c of Nb$_3$Ge first discovered[2] in 1973. In the face of this gross failure to raise the T_c, nonconventional approaches[3] taking advantage of possible strong nonconventional superconducting mechanisms[4] have been proposed and tried. In September 1986, the situation changed drastically when Bednorz and Müller[5] reported the possible existence of percolative superconductivity in $(La_{1-x}Ba_x)Cu_{3-\delta}$ with $x=0.2$ and 0.15 in the 30-K range. Subsequent magnetic studies[6-8] confirmed that high-temperature superconductivity indeed exists in this system. Takagi *et al.*[9] further attributed the observed superconductivity in the La-Ba-Cu-O system to the K$_2$NiF$_4$ phase. By the replacement of Ba with Sr,[8,10,11] it is found that the La-Sr-Cu-O system of the K$_2$NiF$_4$ structure, in general, exhibits a higher T_c and a

sharper transition. A transition width[10] of 2 K and an onset[11] T_c of 48.6 K were obtained at ambient pressure.

Pressure[8,12] was found to enhance the T_c of the La-Ba-Cu-O system at a rate of greater than 10^{-3} K bar^{-1} and to raise the onset T_c to 57 K, with a "zero-resistance" state[13] reached at 40 K, the highest in any known superconductor until now. Pressure reduces the lattice parameter and enhances the Cu^{+3}/Cu^{+2} ratio in the compounds. This unusually large pressure effect on T_c has led to suggestions[8,12] that the high-temperature superconductivity in the La-Ba-Cu-O and La-Sr-Cu-O systems may be associated with interfacial effects arising from mixed phases; interfaces between the metal and insulator layers, or concentration fluctuations within the K$_2$NiF$_4$ phase; strong superconducting interactions due to the mixed valence states; or yet a unidentified phase. Furthermore, we found that when the superconducting transition width is reduced by making the compounds closer to the pure K$_2$NiF$_4$ phase, the onset T_c is also reduced while the main transition near 37 K remains unchanged. Extremely unstable phases displaying signals indicative of superconductivity in compounds consisting of phases in addition to or other than the K$_2$NiF$_4$ phase have been observed by us,[8,14] up to 148 K, but only in four samples, and in China,[15] at 70 K, in one sample. Therefore, we decided to investigate the multiple-phase Y-Ba-Cu-O compounds instead of the pure K$_2$NiF$_4$ phase, through simultaneous variation of the lattice parameters and mixed valence ratio of Cu ions by chemical means at ambient pressure.

The compounds investigated were prepared with nominal compositions represented by $(Y_{1-x}Ba_x)_2CuO_{4-\delta}$ with $x=0.4$ through solid-state reaction of appropriate amounts of Y$_2$O$_3$, BaCO$_3$, and CuO in a fashion similar to that previously described.[8] Bar samples of dimensions $1 \times 0.5 \times 4$ mm^3 were cut from the sintered cylinders. A four-lead technique was employed for the resistance (R) measurements and an ac inductance bridge for the mag-
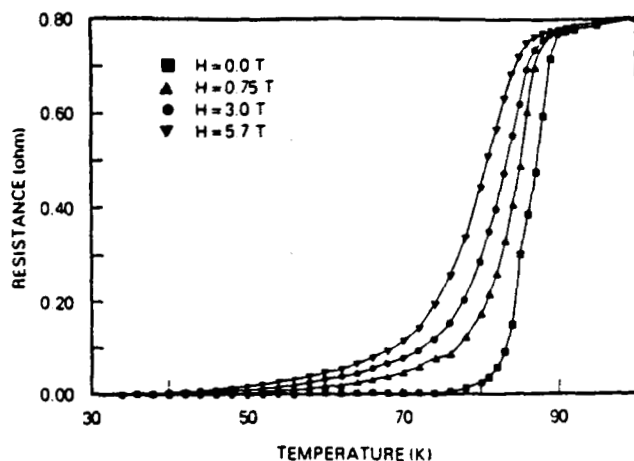
FIG. 1. Temperature dependence of resistance determined in a simple liquid-nitrogen Dewar.

netic susceptibility (χ) determinations. The temperature was measured by means of Au+0.07% Fe–Chromel and Chromel-Alumel thermocouples in the absence of a magnetic field, and a carbon-glass thermometer in the presence of a field. The latter was calibrated against the former without a field. Magnetic fields up to 6 T were generated by a superconducting magnet.

The temperature dependence of R determined in a simple liquid-nitrogen Dewar is shown in Fig. 1. R initially drops almost linearly with temperature T. A deviation of R from this T dependence is evident at 93 K and a sharp drop starts at 92 K. A "zero-R" state is achieved at 80 K. The variation of χ with T is shown in Fig. 2. It is evident that a diamagnetic shift starts at 91 K and the size of the shift increases rapidly with further cooling. At 4.2 K, the diamagnetic signal corresponds to 24% of the superconducting signal of a Pb sample with similar dimensions. In a magnetic field, the R drop is shifted toward lower T. At our maximum field of 5.7 T, the "zero-R" state remains at a T as high as 40 K. Pre-

liminary x-ray powder diffraction patterns show the existence of multiple phases uncharacteristic of the K_2NiF_4 structure in the samples. Detailed analyses are under way.
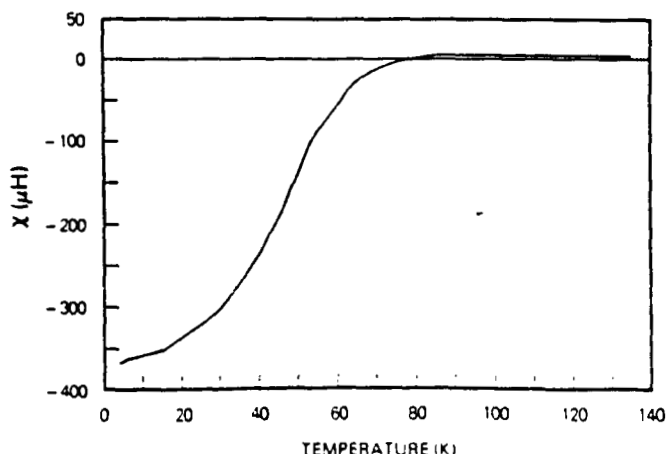
The above results demonstrate unambiguously that superconductivity occurs in the Y-Ba-Cu-O system with a transition between 80 and 93 K. We have determined the upper critical field $H_{c2}(T)$ resistively. If the positive curvature at very low fields is neglected, one gets a value of dH_{c2}/dT near T_c of 3 T/K or 1.3 T/K, depending on whether $H_{c2}(T_c)$ is taken at the 10% or the 50% drop from the normal-state R. In the weak-coupling limit, $H_{c2}(0)$ is thus estimated to be between 80 and 180 T in the Y-Ba-Cu-O system investigated. We believe that the value of $H_{c2}(0)$ can be further enhanced as the material is improved. The paramagnetic limiting field at 0 K for a sample with a $T_c \sim 90$ K is 165 T. Because of the porous and multiphase characteristics of the samples, it is therefore difficult to extract any reliable information about the density of states from the slope of $H_{c2}(T)$ at T_c on the basis of the dirty-limit approximation.

On the basis of the existing data, it appears that the high-temperature superconductivity above 77 K reported here occurs only in compound systems consisting of a phase or phases in addition to or other than the K_2NiF_4 phase. While it is tempting to attribute the superconductivity to possible nonconventional superconducting mechanisms as mentioned earlier, all present suggestions are considered to be tentative at best, especially in the absence of detailed structural information about the phases in the Y-Ba-Cu-O samples. However, we would like to point out here that the lattice parameters, the valence ratio, and the sample treatments all play a crucial role in achieving superconductivity above 77 K. The role of the different phases present in superconductivity is yet to be determined.

FIG. 2. Temperature dependence of magnetic susceptibility.
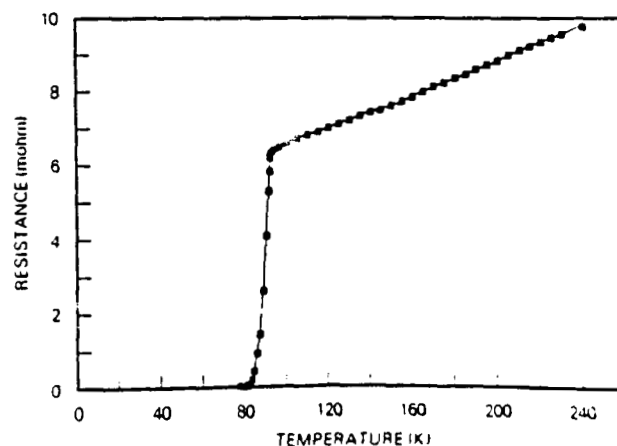
FIG. 3. Magnetic field effect on resistance.

---

[a]Also at the Division of Materials Research, National Science Foundation, Washington, DC 20550.

[1]C. W. Chu, U.S. Patent Application (12 January 1987).

[2]J. R. Gavaler, Appl. Phys. Lett. 23, 480 (1973); L. R. Testardi, J. H. Wernick, and W. A. Royer, Solid State Commun. 15, 1 (1974).

[3]See, for example, C. W. Chu and M. K. Wu, in *High Pressure in Science and Technology*, edited by C. Homan, R. K. MacCrone, and E. Whalley (North-Holland, New York, 1983), Vol. 1, p. 3; C. W. Chu, T. H. Lin, M. K. Wu, P. H. Hor, and X. C. Jin, in *Solid State Physics under Pressure*, edited by S. Minomura (Terra Scientific, Tokyo, 1985), p. 223.

[4]See, for example, J. Bardeen, in *Superconductivity in d- and f-Band Metals*, edited by D. Douglass (Plenum, New York, 1973), p. 1.

[5]J. G. Bednorz and K. A. Müller, Z. Phys. B 64, 189 (1986).

[6]J. G. Bednorz, M. Takashige, and K. A. Müller, to be published.

[7]S. Uchida, H. Takagi, K. Kitazawa, and S. Tanaka, Jpn. J. Appl. Phys. 26, L1 (1987).

[8]C. W. Chu, P. H. Hor, R. L. Meng, L. Gao, Z. J. Huang, and Y. Q. Wang, Phys. Rev. Lett. 58, 405 (1987).

[9]H. Takagi, S. Uchida, K. Kitazawa, and S. Tanaka, to be published.

[10]R. J. Cava, R. B. Van Dover, B. Batlogg, and E. A. Rietman, Phys. Rev. Lett. 58, 408 (1987).

[11]Z. X. Zhao, L. Q. Chen, C. G. Cui, Y. Z. Huang, J. X. Liu, G. H. Chen, S. L. Li, S. Q. Guo, and Y. Y. He, to be published.

[12]C. W. Chu, P. H. Hor, R. L. Meng, L. Gao, and Z. J. Huang, Science 235, 567 (1987).

[13]P. H. Hor, R. L. Meng, L. Gao, Z. J. Huang, and C. W. Chu, to be published.

[14]C. W. Chu, P. H. Hor, and R. L. Meng, unpublished.

[15]According to a report in Renmin Ribao, 17 January 1987.

APPENDIX II

VAPOR TRANSPORT FURNACE PAPER

VAPOR TRANSPORT FURNACE FOR ORGANIC CRYSTALS AND FILMS

Francis C. Wessling[*]
Steven L. Noojin[**]
The University of Alabama in Huntsville
Huntsville, Alabama 35899

Abstract

A vapor transport furnace capable of operating on several different experiment carriers on the Space Transportation System (STS) or on Space Station is described. The furnace itself weighs less that two kilograms excluding its controller. The furnace consists of two concentric aluminum tubes with a vacuum space between them. A quartz ampoule containing the chemicals for crystal growth is placed inside of the inner aluminum tube. Special design considerations allow the furnace to operate at a 413K (140°C) interior temperature with a power consumption of less than three watts when operated in a 293K (20°C) environment. Gold coatings decrease the radiation heat transfer. A special support mechanism between the two aluminum tubes causes the heat transfer by conduction to be inconsequential. Results of thermal analyses are described herein. The design is versatile enough to allow its use in solution crystal growth, polymer reactions and other applications in addition to vapor transport crystal growth. The first flight of three of the furnaces is planned for Get Away Special #105 on the STS.

Introduction

The Consortium for Materials Development in Space at the University of Alabama in Huntsville is one of the NASA centers for commercial development of space and is funded under NASA grant NAGW-812. One of the purposes of the Consortium is to develop materials that have been processed in space for their use in commercial applications here on earth. Several of the projects entail the development of organic electrooptical materials. These can be in the form of optical crystals or optical thin films. Consequently, the Consortium requires a facility capable of multiple use for growing of organic crystals and films. The first Consortium orbital microgravity experiments are intended to occur within a Get Away Special canister onboard the Space Transportation System (STS). It is anticipated that later experiments may occur in middeck lockers, in middeck racks, in an experiment apparatus container, on the Materials Science Lab, in Spacelab and eventually aboard the Space Station. A low temperature furnace has been designed for these applications. It is felt that designing one furnace that may be used in all the possible applications is preferable to designing unique furnaces for each particular application. Thus, the apparatus described in this paper is designed to be suitable for use on all the above carriers. Its first flight is intended to be in Get Away Special #105 (G-105).[1]

---

[*]Associate Director, Consortium for Materials Development in Space, Member AIAA
[**]Graduate Research Assistant

Design Requirements

A furnace designed to be operated on the STS must pass all of the National Aeronautics and Space Administration (NASA) safety requirements. The furnace was intended to fly a large variety of materials. Consequently, the need for triple containment of the experimental chemicals used for crystal and film growth was deemed necessary. The vibrational loads on launch and the impact loads upon landing also influenced the design. The crystals and thin films must survive the reentry and landing without being broken or deformed. Thus, vibrational rigidity, impact resiliency and low thermal losses each significantly impacted the design. The furnace had to be designed to be as compact as possible, light weight, and to use a minimum amount of power for the required temperature because payload space, weight and power were limited on the STS. The overall design requirements were listed in Table 1.

Table 1 Furnace Design Requirements

SAMPLE

    Ampoule Size: 40 mm O.D. x 250 mm long -
                       maximum
    Ampoule Material: quartz
    Processing Temperature: 50°C to 150°C
    Environment Temperature: -10°C to 40°C
    Sample Material: various organics
    Sample Density: 0.8 - 1.2 g/cc
    Sample Size: 100 - 200 mg

MASS AND SIZE

    Furnace mass without controller: < 2Kg
    Furnace and Controller to fit in:
      1. Get Away Special Canister
      2. Experiment Apparatus Container
      3. Middeck Locker
      4. Middeck Rack
      5. Spacelab Rack
      6. Space Station Rack

OPERATIONAL

    Structural Integrity: Withstand launch and
                              landing of STS.
    Sample Protection: Cushioning of crystals and
                           films grown.
    Time to Temperature: < 3 hours
    Power Consumption: < 3 watts @ 140°C
    Sample Temperature Measurement Absolute
      Accuracy: ± 0.2°C
    Sample Temperature Measurement Resolution:
      ± 0.1°C
    Control Setpoint Stability: ± 0.1°C
    Control Setpoint Accuracy: ± 0.2°C
    Maximum Operating Temperature: 200°C

AIAA 26th Aerospace Sciences Meeting
Microgravity Crystal Growth I Session
January 11, 1988   Reno, Nevada

Three such furnaces, each including two samples is planned to fly in G-105. G-105 contains a total of five experiments including 1) a cosmic ray detector, 2) the mixing and demixing of immiscible polymers, 3) electro-deposition of catalyst surfaces and particulate embedded surfaces, 4) optical organic thin film growth, and 5) optical organic crystal growth. Only the cosmic ray experiment is passive. Each of the others requires energy to perform the experiment and also to prevent water-based solutions from freezing when the experiment is not operating. The G-105 battery has a capacity of approximately 1500 watt hours for the entire mission. Energy allocation to the other experiments left a total energy balance of 900 watt hours for the optical organic experiment ampoules. Two ampoules will be placed in each furnace. Each of these ampoules will operate for approximately 100 hours of growth time. Consequently, the total energy loss per ampoule must be extremely low i.e. on the order of approximately 1.5 watts per ampoule or 3 watts per furnace. While these ampoules are operating at a temperature of approximately 140°C the interior of the Get Away Special container could potentially be as low as -10°C under reasonable operating conditions.[2] A temperature of -17.5°C was experienced in Get Away Special-007 which was reported by Rupp at the Get Away Special Experimenters Symposium.[3] G-007 however, had an uninsulated lid. Whereas, G-105 will have an insulated lid.

Furnace Description

The furnace, primarily, consists of two concentric aluminum tubes. A cross section of half of the furnace is shown in Figure 1. The left hand portion is a mirror image of the right hand portion that is shown. The major component parts are shown in Figure 2. This photograph was taken before any of the parts were gold plated or assembled. The outer tube has a diameter of 89 millimeters and a 1.24 millimeter wall. The inner tube has a 51 millimeter diameter and a 1.24 millimeter wall. Within the interior of the inner aluminum tube are two quartz ampoules which con-

tain the materials to be grown. The quartz ampoule is wrapped with a ANSI Type KP heater wire. A thermistor is attached to the center of the ampoule for control purposes. One end of the ampoule holds the sting for crystal growth or a copper flat for growth of optical flats. This end has a controlled energy leak to maintain the temperature of the growth region several degrees lower than the rest of the quartz ampoule. A guard heater and another thermistor are used to regulate the temperature on this end of the ampoule. The ampoule is embedded in a polyimide sponge insulation. This insulation serves to absorb any shock loading due to reentry or hard landing. The crystals and thin films grown in space are protected from mechanical damage by this means. The sponge also serves to thermally insulate the quartz ampoule from the inner aluminum tube.

The outer surface of the inner aluminum tube and the inner surface of the outer aluminum tube are gold plated in order to decrease the radiation interchange between the two tubes. Likewise, the outer surface of the inner tube end caps and the inner surface of the outer tube end caps are gold plated. The region between the two aluminum tubes is evacuated to a pressure of less than 1×10^{-3} millimeters of mercury in order to decrease the conduction and convective heat transfer through the air in that space. In the case of G-105 a vacuum vent line is attached to one of the purge ports on the top of the Get Away Special mounting plate.

In order to decrease conduction losses between the inner and outer aluminum tubes a special mounting mechanism has been devised. This mechanism consists of a set of aramid strands impregnated with high temperature epoxy. The strands form a quadrilateral support mechanism in order to solidly attach the inner aluminum tube to the outer aluminum tube. A photograph of one of the sets of strands is shown in Figure 3. This set has been tensile tested. A total of 6 similar sets are evenly distributed circumferentially around each of the cylindrical tubes. They are
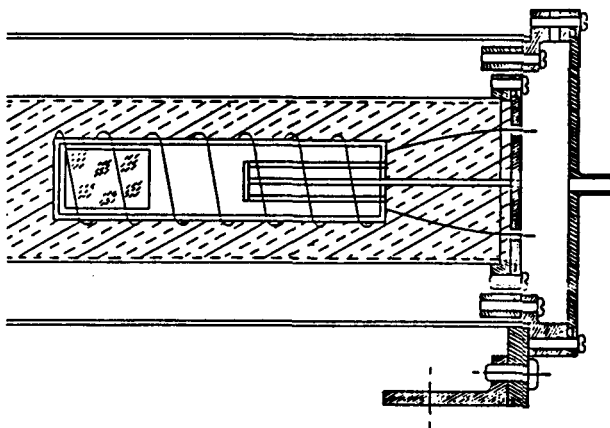

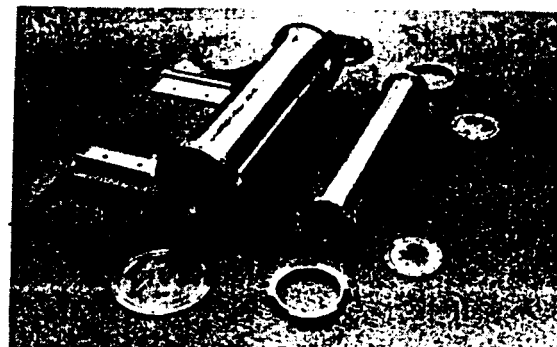Figure 1. Cross section of vapor transport furnace.

Figure 2. Major components of vapor transport furnace.

fastened directly to the inner aluminum tube and its two end support rings. Materials other than aramid such as stainless steel or plastics has been considered for supporting the inner aluminum tube. Unless the support were in tension the cross sectional area of the support would be large enough to cause a considerable amount of conduction heat transfer between the inner and outer tubes. This occurs because the temperature difference between the inner and outer tubes is approximately 100°C. Consequently, the cross sectional area of the support has been made small by putting the aramid strands under tension. The aramid strands have a cross sectional area approximately equivalent to a one-half millimeter diameter strand. A total of 48 of these strands connect the inner aluminum tube to the outer aluminum tube. The strands are oriented in six equal spaces around each end of the tube. They are oriented in such a manner as to prevent torsional and longitudinal vibration of the inner tube. The thermal energy lost through the aramid strands is less than one percent of the total energy lost by the system. The primary means of energy transfer between the inner aluminum tube and the outer aluminum tube is by radiation heat transfer. The polyimide insulation causes a 10°C to 15°C temperature difference between the inner quartz ampoule and the inner aluminum tube. The conduction isolation by use of the aramid strands and the gold coating causes approximately a 100°C temperature difference between the inner aluminum tube and the outer aluminum tube. This shows the benefit of the vacuum jacket and the aramid support strands along with the gold coating.
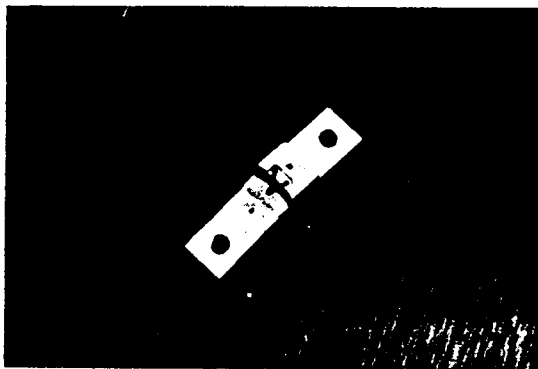

Figure 3. Quadrilateral support mechanism in tensile test jig.

Static tensile tests of the aramid supports showed that one set of four aramid strands was capable of supporting up to 778N (175 lbs) of force when statically applied. The breaking force was more a function of careful attention to geometry rather than to the strength of the aramid itself when the breaking strength was below 778N. The aramid tended to be cut on sharp edges. Consequently, the design included a careful rounding off of each of the edges that the aramid strands passed over. Vibrational tests were accomplished in order to verify the strength of the final assembly.

Each quartz ampoule required a total of eight electrical wires. Four of the electrical wires

were for the two thermistors and four electrical wires were for the heaters. The thermistor wiring was made of copper so as to be compatible electrically with the thermistor. The thermistor was to indicate a temperature change of less than 0.1°C. Consequently, we wanted temperature changes of the wiring to have a small effect on the overall resistance of the thermistor circuit. The heater wires were made from 0.25 millimeter diameter ANSI Type KP wire wrapped around the ampoules. Feeding the wires from the inner quartz ampoule to the outer aluminum tube was done through a series of miniature pin connectors that were epoxied directly into the aluminum end caps. The method of assembly consisted of plugging the wires from the quartz ampoule into the pin connectors in the aluminum cap. Consequently, the quartz ampoule was installed into the tube at the same time that the inner aluminum tube cap was installed. The inner aluminum tube cap had an o-ring groove for a fluorocarbon rubber o-ring to form a vacuum seal. Specifying the wires between the inner aluminum tube and the outer aluminum tube required special care. The ANSI Type KP wire had a low enough thermal conductivity that it did not cause significant conduction heat transfer between the inner and outer tube. Its length was sufficiently long and its diameter was sufficiently small to cause no difficulty. However, the copper wire connections between the inner aluminum tube and outer aluminum tube had to be carefully specified because otherwise the energy loss through those copper wires could double or even triple the total energy consumption of the entire system. A heat transfer analysis showed that the diameter of the copper wire between the inner tube and the outer tube had to be 28 gauge or smaller and the length of the copper wire at least 10 centimeters or else heat losses could be significant. For ease of assembly in the laboratory it was felt that the outer aluminum tube end caps should be installed after the wiring has been completed and checked out. This allowed visual inspection and ease of assembly in a laboratory situation. Consequently, miniature pin connectors were also epoxied into the outer ring of the outer aluminum tube. These then allowed the wires from the inner aluminum cap to be plugged into the pins in the outer aluminum ring. This allowed easy assembly and disassembly of the apparatus in a laboratory and allowed visual and electrical inspection of the connections before the outer aluminum cap was installed. The outer aluminum cap also contained an o-ring groove and an o-ring to complete the vacuum seal.

A temperature depression of the ampoule sting was required for organic deposition. The sting temperature needed to be several degrees to tens of degrees lower than the rest of the ampoule. Several means of allowing energy loss between the inner sting or copper disk and the environment were investigated. The first means used an infrared transparent window in the end cap of the inner aluminum tube and blackening of the surface on the inner portion of the outer aluminum tube end cap. The inclusion of gold plated reflectors would allow view factors between the inner quartz ampoule and the outer blackened surface to be very high. The window of choice was thallium bromoiodide (KRS5). This material had a high thermal radiation transmittance (72%) in the range from 2 microns to approximately 40 microns. The

3

window was rejected as being too uncertain for control of the sting temperature. A second means of causing energy loss was to install a copper wire on the base of the sting or copper disk. This wire was attached to the inner aluminum cap. A second wire was attached from the inner aluminum cap to the outer aluminum cap. A guard heater replaced the excess energy lost to allow temperature control on the sting. An energy analysis of the amount of energy transferred from the sting to the inner aluminum cap and from the inner aluminum cap to the outer aluminum cap showed that the wire between the inner aluminum cap and the outer aluminum cap was unnecessary. That wire increased the amount of energy lost from the system to three times that which was being carried from the sting. Consequently, the wire between the inner cap and the outer cap was omitted. A third means was to attach a thermoelectric cooler to the base of the sting or flat copper plate. A wire similar to the second means connected the base of the thermoelectric cooler to the inner aluminum tube end cap. This cooler acted as a guard heater or cooler as necessary, depending on the applied voltage. This method was to be used for deposition of organic materials when the sting temperature was close to the ambient temperature.

Thermal Analysis

A finite difference thermal analysis was performed on the furnace in order to design some of the thermal features. The high thermal conductivity of the two aluminum containers permitted the analysis to have only 42 nodes because angular symmetry could be assumed. Seventeen of the nodes were in the quartz ampoule; eighteen were in the inner aluminum tube and end cap; six were in the polyimide insulation. The outer aluminum tube was assumed to be at the temperature of the environment. Tradeoff studies were made between various mechanisms for cooling the sting, with the result being the connection of an 18 gauge copper wire serving as a thermal shunt to the cooler environment. This thermal shunt worked adequately to

cool a sting whose temperature was greatly higher than the environment, but failed when the crystal growth temperature occurred close to the environment temperature. Then, a thermoelectric cooling device was placed between the sting and the copper wire.

Three phases of the operation of the furnace were considered: warm-up, steady state operation, and cool down. Simple on-off control was assumed to operate the heaters and coolers. The system heated up from 293K (20°C) to 413K (140°C) in approximately 2 hours. Figure 4 showed the predicted temperature of the polymer source during heat up, steady state operation and cool down. The system cooled from 413K (140°C) to 333K (60°C) in 3 hours with a 293K environment. Steady state power consumption was 2.3 watts with a 293K environment and 2.8 watts with a 253K (-20°C) environment. The thermoelectric cooler was not necessary for these cases. The steady state temperature distribution of the quartz ampoule can be seen in Figure 5 for the 293K case. The thermistor controlling the quartz ampoule temperature was located on its outer surface at the longitudinal center of the ampoule. The energy from the heater windings was evenly distributed between the node with the thermistor and the three nodes on either side of the thermistor. The temperature along the outer tube of the quartz ampoule varied from a high of 413K to a low of 398K as can be seen in the figure. The temperatures of the source of the organic material varied from 408K to 412K as can be seen in Figure 6. The left most node shown in the figure was a quartz ampoule node. The temperature of the sting and its support can also be seen on the figure, with the sting at the desired temperature of 409K (136°C) and the temperature decreasing linearly to a value of 399K at the end of the ampoule.

The temperature distribution throughout the ampoule could be varied by selecting the placement of the thermistor, the distribution of the windings of the heater coils, and the control of the sting temperature. The thermal analysis showed
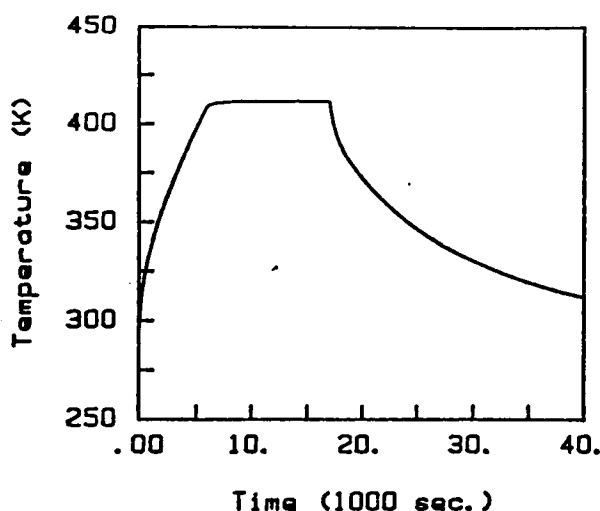
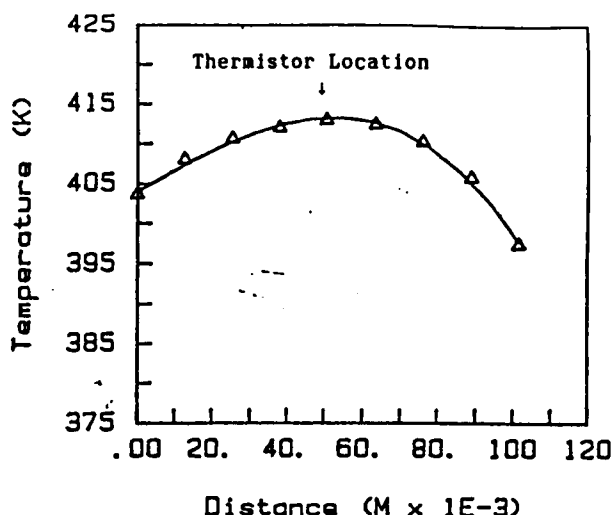Figure 4. Source tip temperature during warm-up, steady state, and cool down operations.

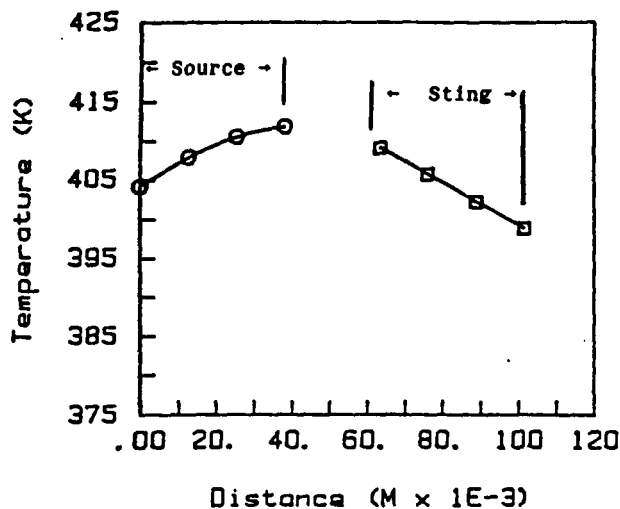Figure 5. Quartz ampoule longitudinal temperature distribution.

4

Figure 6. Quartz ampoule source and sting longitudinal temperature distribution.
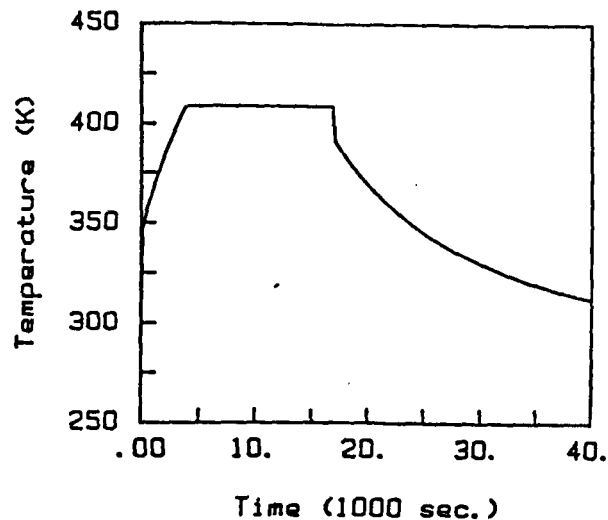

Figure 7. Sting tip temperature during warm-up steady state, and cool down operations.

the adequacy of the design. Laboratory tests will determine the final configuration of the windings.

Figure 7 showed the predicted temperature of the sting during warm up, steady state operation, and cool down. Comparison of the temperature of the source (Figure 4) to the temperature of the sting showed the slower time response of the more massive source. The sting heated up more quickly than the source. This would cause no growth of crystals on the sting until the steady state temperature of the sting was attained. This was the desired mode of operation.

The temperature response was not so benign on cool down. A fast change in temperature was caused by the low thermal capacitance of the sting and by the copper thermal shunt between the sting and the inner aluminum tube. The temperature of the sting dropped much more quickly than the temperature of the source. The sting temperature dropped approximately 0.3°K/S when the sting heater was initially turned off. This caused the temperature of the sting to fall almost 18K below the temperature of the source. This was undesirable as it could allow a high deposition rate onto the sting. Consequently, instantaneous shut down appeared undesirable.

Thus, the furnace shut down sequence was specified to maintain the temperature of the sting several degrees cooler than the source. This would allow the deposition rate to slowly decrease as the temperature of the source, and the vapor pressure of the source decreased. The scheme was to turn off the source heater and require the temperature of the sting heater to follow the temperature of the source within 3K.

Conclusion

The vapor transport furnace described herein has been developed for space flight. Its geometry allows installation on several different experiment carriers on the STS and on Space Station. The furnace was originally designed for vapor transport crystal growth or thin film growth. However, its design is flexible enough to allow its application to solution crystal growth and also to polymer interactions. Power consumption has been carefully controlled so that two crystal growth ampoules may be heated to 413K with a steady state power consumption of less than three watts when operated in a 293K environment. The furnace heats up to this temperature within 2 hours. The first flight of the furnace is planned for Get Away Special #105 in the Consortium for Materials Development in Space microgravity flight experiment program.

References

1. F. C. Wessling, "Phase Partitioning, Crystal Growth, Electrodeposition and Cosmic Ray Experiments in Microgravity." Proceedings of the 1986 Get Away Special Experimenters Symposium, NASA-CP-2438, pps. 15-22.

2. D. Butler, "Get Away Special Thermal Design Summary." NASA X-732-83-8, July 1983.

3. C. C. Rupp, "Marshall Amateur Radio Club Experiment (MARCE) Post Flight Data Analysis." Proceedings of the 1986 Get Away Special Experimenters Symposium, NASA-CP-2438, pps. 149-156.

5